Graduate School ETD Form 9
(Revised 01/14)

PURDUE UNIVERSITY
GRADUATE SCHOOL
Thesis/Dissertation Acceptance

This is to certify that the thesis/dissertation prepared

By Lujie Ye

Entitled
TOWARDS COMMERCILIZATION OF SELF-HEALING TECHNOLOGY IN EPOXY COATINGS

For the degree of Master of Science in Mechanical Engineering

Is approved by the final examining committee:

Alan Jones

Jing Zhang

Likun Zhu

To the best of my knowledge and as understood by the student in the *Thesis/Dissertation Agreement. Publication Delay, and Certification/Disclaimer (Graduate School Form 32)*, this thesis/dissertation adheres to the provisions of Purdue University's "Policy on Integrity in Research" and the use of copyrighted material.

Alan Jones

Approved by Major Professor(s): _____

Approved by: Jie Chen 06/20/2014

Head of the Department Graduate Program Date

TOWARDS COMMERCIALIZATION OF SELF-HEALING TECHNOLOGY IN EPOXY COATINGS

A Thesis

Submitted to the Faculty

of

Purdue University

by

Lujie Ye

In Partial Fulfillment of the

Requirements for the Degree

of

Master of Science in Mechanical Engineering

August 2014

Purdue University

Indianapolis, Indiana

ACKNOWLEDGMENTS

First of all, I would like to show my deepest gratitude to my advisor, Dr. Alan Jones, a respectable and resourceful scholar, who has provided me with valuable guidance in every stage during my research and thesis preparation. Without his enlightening instruction, impressive kindness and patience, I could not have completed my thesis. His keen and vigorous academic observation enlightens me not only in this thesis but also in my future study.

I would like to extend my thanks to Dr. Jing Zhang and Dr. Likun Zhu. Their critical suggestions and advises are really valuable my research. My sincere appreciation also goes to the staffs in Purdue School of Engineering of Technology of IUPUI. Their high efficiency and kindness always make things easier and make me feel at home.

Last but not least, I would like to thank my husband and all my friends, for their encouragement and support.

TABLE OF CONTENTS

LIST OF FIGURES

Figure Page

Appendix Figure

ABSTRACT

Ye, Lujie. M.S.M.E., Purdue University, August 2014. Towards Commercialization of Self-healing Technology in Epoxy Coatings. Major Professor: Alan Jones.

This work is focused on developing viable self-healing coatings, especially considering the viability of the coating in a commercial context. With this in mind, finding low cost healing agents, with satisfactory healing and mechanical properties as well as adapting the healing system for use in coatings was required. Seven potential healing agents were evaluated and an air-drying triglyceride (linseed oil) was identified as the candidate healing agent. Different encapsulation techniques were evaluated and urea-formaldehyde microcapsules were chosen as the candidate encapsulation technique. Self-healing coatings were fabricated using urea-formaldehyde encapsulated linseed oil. EIS, SEM and TGA technologies were used to evaluate the mechanical performance, corrosion resistance, and self-healing performance.

1. INTRODUCTION

From 1994 to 1999 there were a total 1,564 oil and gas transmission pipeline accidents in United State and approximately 385 of them are due to corrosion [1]. In 2001 the U.S. Federal Highway Administration estimated the annual cost of corrosion for the United States to be $276 billion or 3.1% of GDP [2]. The numbers above are only the direct economic costs of corrosion, which include material preparation and the labor costs for prevention and repair. There are also a large number of indirect economic costs associated with corrosion, which include plant downtime, loss of product, loss of efficiency, contamination and overdesign. Those costs are harder to estimate and they may even have a larger impact than direct costs. Besides economic costs, corrosion also takes a significant cost in human life and safety. Oil leakage caused by corrosion may contaminate drinking water and therefore impair human health. Serious corrosion may even cause explosion, thus resulting in significant life loss. Due to all those reasons, there are more and more stringent federal and state regulations toward corrosion leaks. More research in corrosion science and engineering is therefore desperately needed. The most common way to protect materials from corrosion is with coatings, including organic (paint), ceramic and metallic coatings. During use, micro-cracks form in the coating resulting in exposure to the environment, which can lead to catastrophic failure of critical components. A low-cost self-healing system can significantly extend the service life of coatings and the components they protect.

1.1 Corrosion

Corrosion is a chemical or electrochemical reaction between a metal and the surrounding. Corrosion will lead to a deterioration of the metal and its properties [3]. All forms of corrosion, with the exception of high-temperature corrosion, occur through

the action of the electrochemical cell as shown in Figure 1.1. All corrosion cells include an anode where oxidation and metal loss occurs, a cathode where reduction occurs, electrolytic paths between the anode and cathode through which electronic and ionic current flows, and a potential difference that drives the cell. The general reaction on the anode side is of the form

$$M- > M^{n+} + n^{e-} \tag{1.1}$$

where M represents a corrosive metal, n is the number of electrons being transferred and $e-$ is an electron. For example if the metal is iron, equation (1.1) becomes,

$$Fe- > Fe^{2+} + 2e^{-} \tag{1.2}$$

The resultant ferrous ion will leave the oxide-free metal surface and enter into electrolyte solution. Electrons will be left in the metal. This type of reaction is a reversible reaction. The accumulation of the electrons in the metal will lead to the reverse of the reaction, which retards the dissolution of ferrous ion. In an acid solution, the remaining electrons will react with hydrogen ions by decreasing the oxidation state of hydrogen from +1 to 0. This reduction reaction is shown in equation (1.3)

$$2H^{+} + 2e^{-}- > H_2 \tag{1.3}$$

The reduction reaction consumes the electrons generated in the oxidation reaction, which leads the oxidation reaction to continue and produce more metal ions, dissolve more metal ions into solution and continue corrosion of the metal. In a neutral solution, the concentration of H^+ is too low for the oxidation to continue at a high rate. The oxygen dissolved in the solution will participate in reduction at the cathode. The reaction at the cathode is $O_2 + 2H_2O + 4e^{-}- > 4OH^{-}$.

While the underlying mechanism for corrosion is the same, there are different ways of categorizing the corrosion depending on the physical effects and the conditions of the corrosion. For example in uniform corrosion the entire surface is corroded simultaneously, while in localized corrosion (including pitting and crevice), corrosion usually

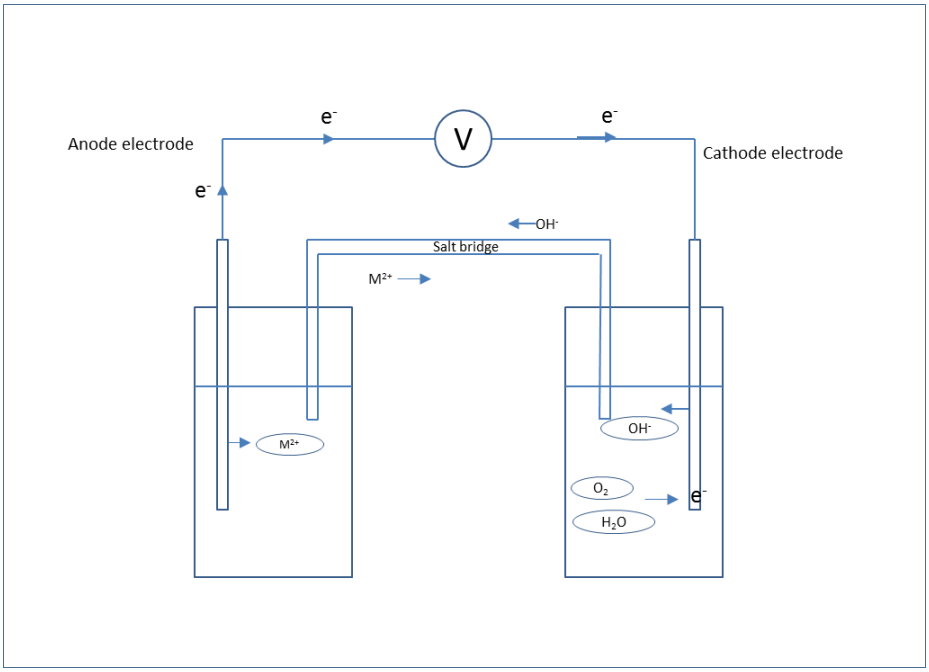

Figure 1.1. Electrochemical Cell Sketch

occurs predominantly at one specific location. Galvanic Corrosion occurs when two electrochemically dissimilar metals are located together in a corrosive electrolyte. Environmental cracking is the result of environmental effects like chemical, temperature and stress-related conditions. The typical environmental cracking types are Stress Corrosion Cracking (SCC), corrosion fatigue, and hydrogen-induced cracking. The impurities in the metal near grain boundaries, and the selective corrosion of a specific element in an alloy will lead to intergranular corrosion and de-alloying respectively. Other effects that are commonly associated with corrosion are erosion, cavitation and fretting [4]. An example of the different classifications of corrosion is shown in Figure 1.2.

1.2 Corrosion Protection

There are many ways for accounting for or preventing corrosion. While a detailed description of all of the methods of corrosion protection is beyond the scope of this

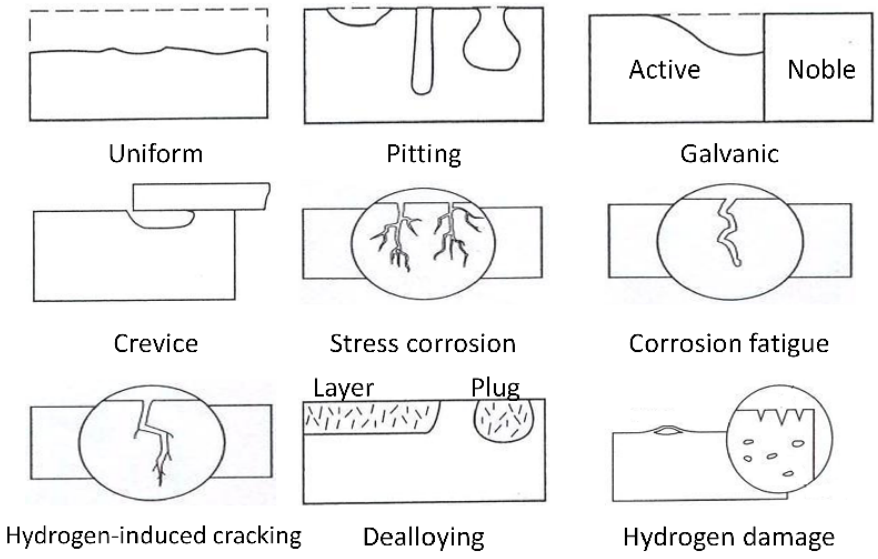

Figure 1.2. Different Forms of Corrosion. From Ref. [4]

thesis, a brief description of the most commonly used techniques will be provided here.

Choosing materials that are inherently corrosion resistant or creating designs that include a corrosion allowance is one of the best ways of preventing the effects of corrosion. Unfortunately materials with high corrosion resistance are usually expensive and including a corrosion allowance results in heavier, more expensive designs. Alternatively, corrosion protection methods can be used to protect standard non-corrosion resistant materials. Example corrosion protection methods include inhibitors, cathodic protection, and coatings.

Inhibitors are chemicals that prevent corrosion by forming a protective coating due to the reaction of the inhibitors with solution at the corroding surface. Chromate, Nitrites, benzoates, borates and silicates [5–7]are inhibitors for steel corrosion protection. Recently, many new inhibitors like Zenthoxylum alatum [8], Bis (benzimidazol-2-yl) disulphide [9] have been discovered to have significant corrosion resistance effectiveness. Many inhibitors are toxic, expensive, and they are consumables, so that inhibitors are best used in recirculation systems. However, inhibitors

still play an important role in many corrosion-control strategies. Inhibitors are commonly used in areas such as industrial cooling water, post-service cleaning to remove rust on metal parts, and transportation of crude oil and refining processes.

Cathodic Protection is a method of preventing corrosion of a target material by forcing the material to become a cathode. This is accomplished by joining the target material with a sacrificial anode. The sacrificial anode will corrode, and provide electrons to the protected material, preventing it from undergoing the oxidation process. Another method of forcing the material to become a cathode is through forcing a current. The required current for forced-current Cathodic Protection can be determined from the cathodic polarization-current density diagram. The corrosion protection performance of forced-current Cathodic Protection is effective but sometimes impractical, especially for aggressive acid solutions with high corrosion rates [4]. On the other hand, an example of sacrificial anodes used in the Cathodic Protection of iron in seawater are zinc aluminum, and magnesium alloys [4]. Sometimes Cathodic Protection is combined with coatings to supplement for each other. The imperfections (pinholes, voids, physical damage, flaws and so on) on the coating face the highest risk of corrosion. Through applying cathodic protection, the weak part of coating will attract the applied cathodic current to concentrate, which reduces the corrosion rate by cathodic polarization of the substrate metal. Providing sufficient current or sacrificial anodes for large structures is not always feasible and can result in large continuous costs for corrosion protection.

Protective coatings can either be metallic, ceramic, or organic. Example metallic coatings include hot-dipped zinc, aluminum-zinc [4] coatings, which act both as a corrosion resistant physical barrier and sacrificial anode. Electroplated chromium provides corrosion protection through the hard chromium oxide. Compared with organic coatings, metallic coating are difficult to apply and cannot typically be applied in the field [4].

Ceramic coatings are typically inert and are very resistant to corrosive environments and chemicals. Unfortunately, high temperatures are required to apply a ce-

ramic coating. Brittleness is another limitation of typical ceramic coatings. The requirement of high temperature and the resulting brittleness of the ceramic coatings limit the application of ceramic coatings in many fields.

Organic coatings are the most common coating type, especially when the cosmetic appearance of the system is important. Commonly used coatings are alkyd, epoxy ester, and polyester urethane. All of these are liquid-applied organic coatings. They can be applied to small or large parts and are commonly applied in the field [4]. The application can be done at room temperature and little specialized equipment is needed. The corrosion protection for metal in a mildly corrosive atmosphere is effective, with the corrosion rate less than 1.3mm/yr(50mpy) [4]. While cracks in the coating, sometime even micro-cracks, can expose the substrate to the corrosive environment and result in the corrosion of the metal and eventual failure of the system. This potential risk makes organic coating an ideal candidate for incorporating self-healing technology. Self-healing coatings should repair crack automatically and greatly extend the working life of the coating. The development of self-healing organic coatings is the focus of this thesis.

1.3 Types of Self-Healing

There are three different types of self-healing materials (shown in Figure 1.3): Intrinsic self-healing, Vascular self-healing and capsule-based self-healing

Intrinsic self-healing materials do not use healing agents to repair the crack or damage. Instead, they repair damage through their intrinsic nature due to the reversibility of the matrix polymer [11]. The intrinsic self-healing process is achieved through chemical and physical interactions including hydrogen bonding, chain mobility and thermal reactions [12]. Example intrinsic self-healing materials are Diels-Alder (DA) and retro-Diels-Alder (rDA) reactions based. Reference [13] and [14] provide example of intrinsic self-healing materials. In general, intrinsic self-healing materials have a very narrow scope for application. The material is necessarily very compliant,

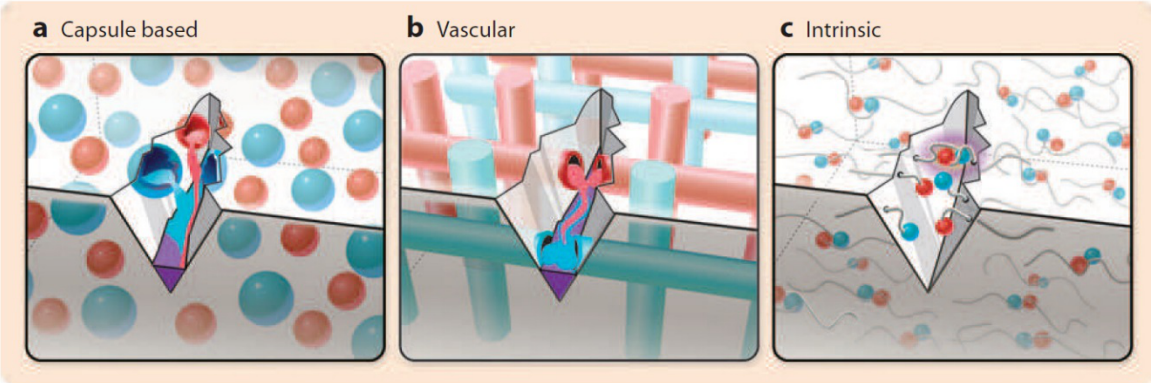

Figure 1.3. Visualization of *a*) Capsules Based *b*) Vascular Based and *c*) Intrinsic Self-healing. From Ref. [10]

which limits its use in structural applications requiring any degree of stiffness, and the suitability of intrinsic self-healing coatings has not been evaluated but is expected to be rather poor due to lack of adhesion, low toughness, and poor surface finish of these materials.

Vascular self-healing materials imitate biological systems utilizing a vascular network to facilitate healing [10]. The healing agent is inside a network of channels in the host material. The channels can be connected to each other in one dimension, two dimensions or three dimensions. When external damage cause cracks the channel is ruptured and triggers the self-healing process. In this case, the healing agent is released from the broken channel and fills the crack. This type of system allows the network of channels to be refilled with additional healing agents to allow the self-healing mechanism to continue working after a damage event.

Capsule based self-healing material is another biological inspired system where damage can be repaired automatically. The concept of capsule based self-healing materials is to embed microcapsules filled with healing agents into the host material. When damage occurs, microcapsules will be broken and release the healing agent. The polymerization of the healing agent (which may need a catalyst) will lead to

the formation of a film to prevent crack propagation or future damage. Figure 1.4 indicates the design of self-healing materials.

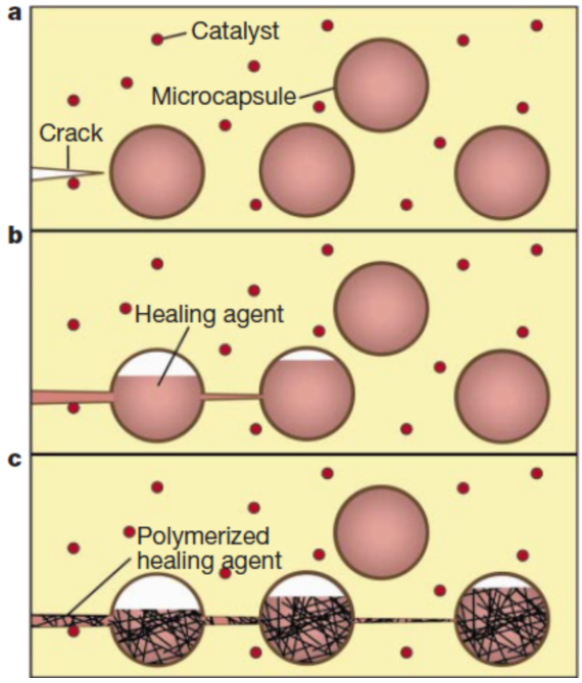

Figure 1.4. Schematic of Self-healing Process. From Ref. [15]

S. R. White et al. developed the first structural polymeric material with the ability to automatically heal cracks with dicyclopentadiene (DCPD) and Grubbs catalyst in 2001 [15]. The healing system consisted of hollow microcapsules filled with a healing agent dispersed throughout the polymer matrix. As a crack propagates through the polymer matrix, the microcapsules are ruptured, allowing the healing agent to flow into the crack plane. Polymerization of the healing agent by ROMP (ring-opening metathesis polymerization) occurs when the healing agent comes in contact with an exposed catalyst particle on the fracture plane. This process can be found in Figure 1.4.

Following Whites research, self-healing has been extensively studied. Urea-formaldehyde (UF) [16–21], melamine-formaldehyde (MF) [22,23], melamine-urea-formaldehyde(MUF) [1], phenol-formaldehyde (PF) [24], polyurethane(PU) [25], and oracrylates [26] as a

polymer shell microencapsulation techniques were developed. They are all in situ formation techniques. In our work, UF, MUF, PF and PU encapsulation techniques were tried. The mechanism and encapsulation process will be discussed in experiment section. Based on above microcapsules encapsulation methods, self-healing system with DCPD (Grubbs as catalyst) [15, 27], ENB blend (Grubbs as catalyst) [28], Solvent: epoxy resin (Deta as catalyst) [29], HOPDMS/PDES (DMDNT as catalyst) [30] or Linseed oil [31] as healing agent and epoxy as matrix material was created. Other healing agents like silyl ester [32], hexamethylene diisocyanate [33] can also be found in literature.

There are four types of capsule based self-healing systems (shown in Figure 1.5). The first generation shows the capsule-catalyst method in which the healing agent is put into capsules as a liquid and a catalyst that is dispersed throughout matrix material as described above [15].

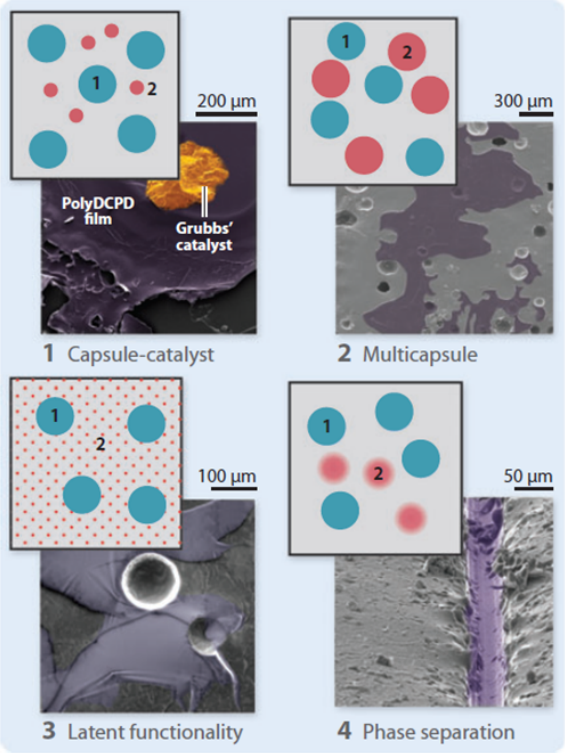

Figure 1.5. Four Types of Capsule-based Self-healing Systems. From Ref. [10]

Figure 1.5.2 [19] shows the multicapsule method in which both the healing agent and the polymerizer are encapsulated. It is the second generation of capsule based self-healing material. The third system, latent functionality, is displayed in Figure 1.5.3 [29]. In this system, the healing agent is encapsulated or dispersed as particles while the polymerizer is residual reactive functionality in the matrix or an environmental trigger. This system uses a latent function of the matrix, that is to say it uses a tertiary function of the matrix to facilitate the reaction in which the matrix acts as the catalyst to cure the healing agent. Figure 1.5.4 shows the phase separation system in which either the healing agent or the polymerizer is phase-separated in the matrix material [34].

The capsule-based healing systems are good candidates for creating self-healing coatings to protect materials from corrosion. Figure 1.6 shows an application of a capsule-based, self-healing coating that has been applied to steel and then scored. Figure 1.6.a shows the steel substrate scored with no coating, and Figure 1.6.b shows the scored steel substrate with applied coating.

Figure 1.6 c, d shows a micro-enhanced view of the Figure 1.6a, b. These images were taken after a steel substrate, one without a capsule-based self-healing coating (which appears in Figure 1.6a, c) and a steel substrate with the coating (which appear in) Figure 1.6b,d). The specimens were immersed in a salt water bath for 120 hours. It can be observed from the Figure 1.6 that the control specimen with no coating had severe corrosion on the surface and in the scored area. However, the specimen with the coating displays no evidence of rust [34]. This is a good example of how a capsule-based self-healing coating could be applied to preserve the life of a component.

1.4 Research Opportunities

1.4.1 Self-healing Coating

Self-healing coating is a relatively new research topic. Cho et al [34] developed a phase separated self-healing coating. They utilized a vinyl ester as a healing agent and

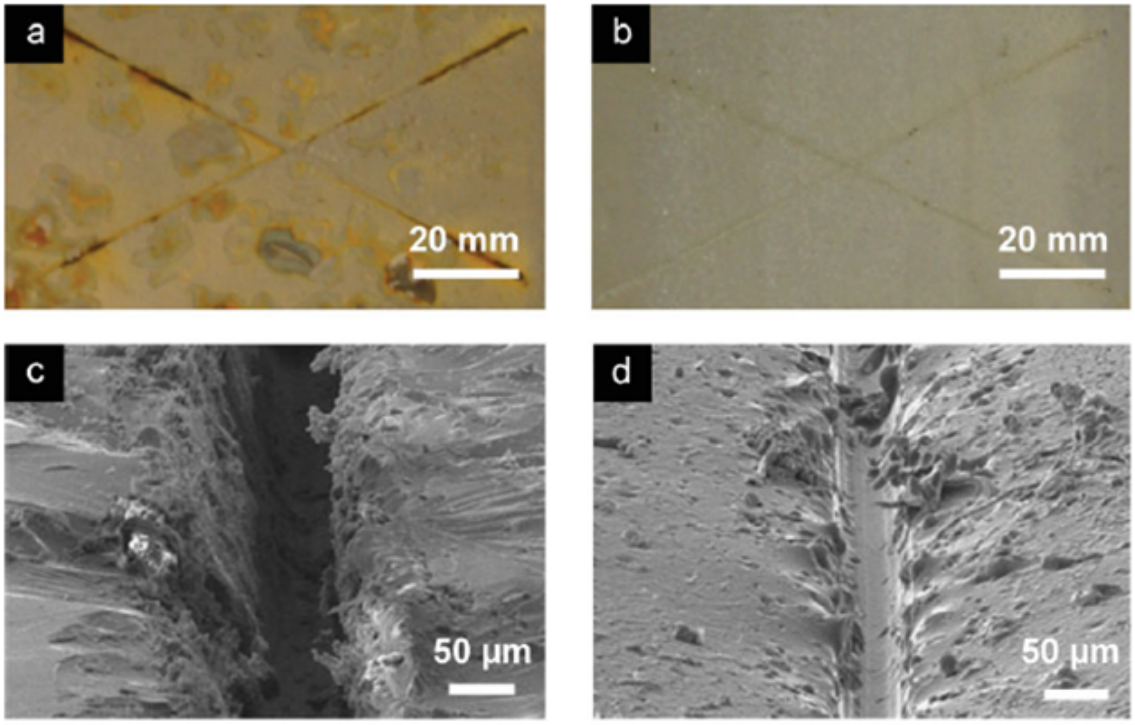

Figure 1.6. The Corrosion Resistance of Coating with or without Capsules. From Ref. [34]

the performance was evaluated by visual inspection. Kowalski et al [35] developed an intrinsically conducting polymer coating, polypyrrole doped with molybdate on carbon steel, and evaluated the performance by open circuit potential. Aramaki et al [36] developed a ultrathin self-healing coating by modified 16-hydroxyhexadecanoate ion self-assembled monolayer (SAM) on a passivized iron substrate to protect the passive film from breaking down in NaNO3 solution. Yabuki developed TiO2 particles based self-healing coatings for alloy substrate. A TiO2 particles based self-healing coating was developed by applying casein as pH-sensitive organic agents [37] to protect magnesium alloy substrate. When changing pH from 12 to 5, a film formed by TiO2 and casein were observed by SEM. In his future work, TiO2 particles based self-healing coating was also applied to protect aluminum alloy from corrosion of seawater [38]. An alternative idea in designing self-healing coating is: instead of embedding mi-

crocapsules into coating, porous coating was designed to prepare pore for corrosion inhibitor [39]. From the perspective of assessment technology, lots of electrochemical techniques were applied to measure the healing efficiency of self-healing coating and study the healing mechanism as well. Gonzalez-Garcia [40] first time used SECM to study the early stage of corrosion activities in the self-healing coating when it was damaged. The self-healing coating is the epoxy coating embedded with silyl-ester as healing agent. His work demonstrated the effectiveness of the silyl ester based self-healing coating through the sufficient silyl ester release and silyl esters inhibition. Neema et al. [41] generated acrylic-Silicone interpenetrated polymer network (IPN) for high temperature application. Self-healing acrylic-Silicone IPN was achieved by embedding UF microcapsules with epoxy resin as healing agent and melamine-based hardener as catalyst. SVET and EIS were applied to evaluate the self-healing coating performance. The corrosion protection performance evaluation methods will be demonstrated in detail later.

With the development of self-healing coating, a simpler one-part self-healing coating was designed. This kind of self-healing coating only requires one part-capsulized healing agent, with no need of catalyst. Those healing agents polymerization are environmental simulated. One example of one-part, catalyst-free healing system was developed by Jadhav et al [24]. Linseed oil was used as healing agent and phenol-formaldehyde was the microcapsule shell. The healing performance of was inspected by visual inspection. Huang et al [33] developed a one-part self-healing coating embedded by PU microcapsules containing hexamethylene diisocyanate (HDI) with no need of catalyst. Besides, a facile way to synthesize polyurethane by using commercial methylene diphenyl diisocyanate (MDI) as prepolymer was utilized. The performance of the developed self-healing coating was also assessed by visual inspection. Another emerging self-healing coating design is layer by layer coating. Kumar [42] first used primer-microcapsule-primer-topcoat four layers self-healing coating to increase the adhesion of self-healing coating. Such kind of self-healing coating based on LbL assembled technologies [43–46] is continuously being developed.

1.4.2 Corrosion Protection Performance Evaluation

The traditional way of evaluating the corrosion rate is by weight loss measurement [4], which usually takes several days. Since corrosion is an electrochemistry process, an alternative and currently popular way to measure the corrosion rate is through the electrochemical polarization [4]. Simmons [47] and Skold [48] found that the corrosion rate is inversely proportional to polarization resistance. This observation was later verified [47–49] and developed [50, 51] as an accelerated measurement for corrosion rate and corrosion monitoring. Recently, lots of electrochemical polarization based electrochemical technologies were introduced to evaluate the self-healing process and corrosion protection performance of self-healing coatings. The most common electrochemical technologies for corrosion detection and evaluations are Tefel extrapolation based Potentiodynamic Polarization (PP) [52–55], Linear Polarization Resistance (LPR) [56], and polarization resistance based Electrochemical Impedance Spectroscopy (EIS) [32, 38, 39, 41, 57]. Those two technologies are used to measure average corrosion resistance. In order to measure the localized corrosion rate, which is corrosion of a small area, other electrochemical techniques were introduced. Scanning vibrating electrode technique (SVET) measures current density by using a vibrating probe. The resulting signal gives the information of ion distribution, which provides information of corrosion kinetics. SVET was also applied together with Scanning ion-selective electrode technique (SIET) [58, 59] or localized electrochemical impedance spectroscopy (LEIS) [60] to gain both the information of local ion distribution and reactivity during healing process of coated parts, providing information of the mechanism of localized corrosion. An emerging and promising electrochemical technique is Scanning Electrochemical Microscope (SECM). SECM offers the possibility of detecting local defect both on organic and metallic surface through assessing locally electrochemical reaction at anodic and cathodic sites [61, 62].

Besides electrochemical technology, surface morphology analysis is also widely used to assess the self-healing performance of the coatings. The advantage of surface

morphology measurements is that they provide visual inspection and quick assessment of corrosion status. Usually, they are applied together with electrochemical techniques to achieve both qualitative and quantitative assessment. Common used surface morphology analysis techniques are Optical Microscopy [63], Scanning Electron Microscope (SEM) [24, 33, 42, 63, 64] and Confocal Laser Scanning Microscopy (CLSM) [64]. Besides the surface morphology evaluation, CLSM can also provide 3D image of a specimen, which measures the depth of the corrosion. This feature is valuable when studying pitting and crevice corrosion. Energy-dispersive X-ray (EDX), X-ray Photoelectron Spectroscopy (XPS) are available to analyze chemical composition during self-healing process, which contribute to the study of self-healing process mechanism and kinetics.

1.4.3 Research Objective

It has been more than ten years since the capsule based self-healing concept was originally introduced. However, most of the research was focusing on finding new and more effective healing agents to improve the corrosion protection performance of the self-healing system. There was no work related with mechanical properties comparison between the self-healing coating system and the coating system with no self-healing. On the other side, although the long time existence of self-healing technology, there is no commercial product on the market. In order to transition the self-healing coating technology from laboratory to commercial use, mechanical properties of self-healing coating need to be evaluated. At the same time, an affordable self-healing system with long time stability need to be developed to meet the need of the market.

2. EXPERIMENTAL PROCEDURE

The typical evaluation of a self-healing coating consisted of fabricating the coating material, applying the coating material to a substrate, evaluating the mechanical performance of the coating or damaging the coating, and monitoring the corrosion protection capability of the damaged coating. In addition to these procedures, additional experiments were performed to aid in the selection of candidate healing systems. The details of the experimental procedures and methods are outlined in the following sections.

2.1 Specimen Preparation and Coating

According to the standards for steel surfaces distributed by the Association of Corrosion Engineers(NACE), the steel surfaces need to be cleaned by sand blasting or steel shot blasting with white metal blast (NACE No. 1 standard) being preferred when preparing surface of steel. For this work, the steel used is 1074/1075 spring steel, which was purchased from McMaster-Carr (part number $9074K13$) . The steel is unpolished and cold rolled with the size of 2 inches wide and 5 feet long. The steel was prepared by cutting it into 23 inch pieces and sanding the surface using a DeWalt Electric Orbital Sander with different grits to prepare the surface of the steel.

After getting the steel surface ready, an epoxy coating is applied onto the surface of the steel. The coating process followed protocol ASTM D823 and the coating thickness was targeted between 100-200 micrometers. A custom made Doctor Blade shown in Figure 2.1 was used to get an even and uniform coating and control the thickness of the coating. The final coating thickness could be changed by adjusting the micrometer heads on the top of the doctor blade fixture (Figure 2.1).

The epoxy coating used for all experiments is a two part epoxy system consisting of a resin and hardener. The two parts need to be mixed and allowed to cure for a certain period, typically $12 - 48$ hours, depending on the temperature cure cycle. In this case, 12 weight percentage of Diethylenetriamine (DETA) was used as the hardener in 828 epoxy. The epoxy was weighed and an appropriate amount of DETA was added to the epoxy. After stirring the mixture for approximately one minute, it was degased for 15 minutes using a vacuum chamber to remove dissolved air. For the case of self-healing specimens, the microcapsules were added to the degassed epoxy and the mixture was gently stirred to distribute the microcapsules. In the case of neat epoxy coatings used for control specimens the degassed mixture was used without any additional stirring. The epoxy coating, with or without capsules, was applied to one end of the prepared surface of the steel specimen. The Doctor Blade was then slid over the top of the specimen to evenly distribute the coating material. A clamping table was created to securely hold the specimen at the very ends to facilitate creating a uniform coating. After coating, the specimens were transported to an oven and heated to 30 °C for 24 hours. The specimens were then removed from the oven and allowed to cure at room temperature for another 24 hours. The total cure time for a specimen was forty-eight hours.

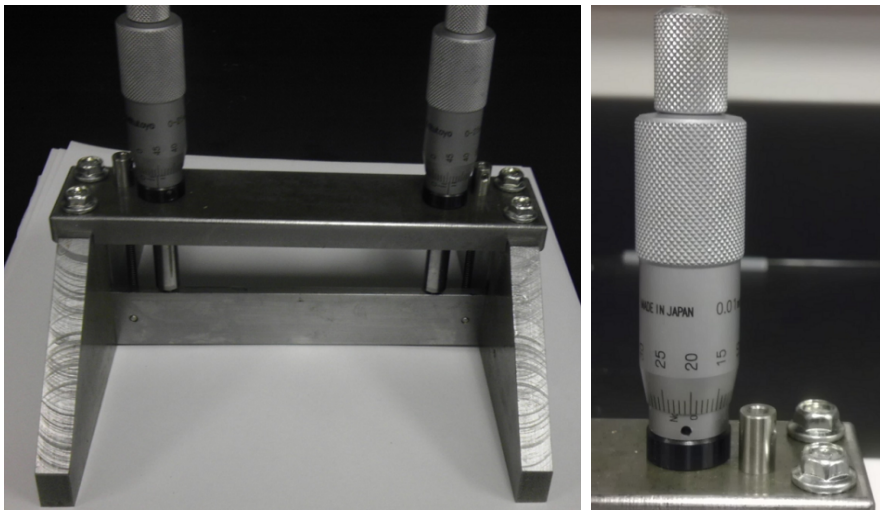

Figure 2.1. The Design of Doctor Blade Fixture and Micrometer Head

2.2 Injection Test

The injection test provided a method of evaluating possible healing chemistries. This type of test may not represent the actual healing performance of the self-healing system, but allows the evaluation of healing candidate materials with respect to adhesion to the coating material, crack filling, and how well the coated substrate resists corrosion. This test does not include the added complexity of delivery methods, for example phase separated or microcapsule systems.

The injection test is performed by manually injecting approximately 2 ml of the healing chemistry onto the crack plane using a syringe (refer to Figure 2.3). The process of performing an injection testing is as follows:

a) Create a sharp pre-crack by drawing a razor blade across the surface of the epoxy coated specimen.

b) Inject the potential healing chemistry into the damage site created by step a.

c) Submerse half of the specimens in room temperature 5% salt water and allow the other half of the specimens to rest in air for 2 hours at room temperature. After the 2 hours resting period the specimens were then submersed in room temperature 5% salt water.

d) Each specimen was periodically removed and photographed every 1 hour, 2 hours, 12 hours, 2 days and 7 days to evaluate corrosion protection performance of the candidate healing system. Electrochemical Impedance Spectroscopy (EIS) tests were also used to evaluate the corrosion protection performance of those healing chemistries. The potential healing chemistries under comparison are listed in 2.2. One feature identified early in this work was the desire to reduce the cost and complexity of the healing system. For this reason, healing agents that required minimal or no catalysts were primarily chosen for this work.

Potential healing chemistry	Supplier
Tung oil	Sigma Aldrich
3-aminopropyl triethoxysilane	Sigma Aldrich
3-mercapto trimethoxysilane	Sigma Aldrich
Raw linseed oil	Sigma Aldrich
Boiled linseed oil	Klean Strip
Dimethylethanolamine	Sigma Aldrich
Hexamine	Sigma Aldrich

Figure 2.2. Potential Healing Chemistries Evaluated With the Injection Test

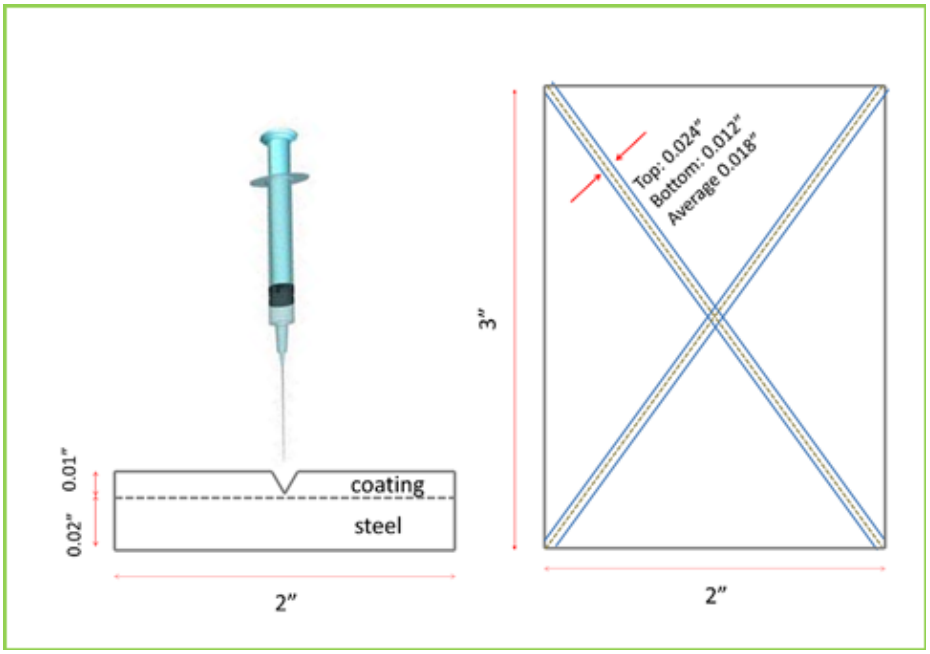

Figure 2.3. The Section and Planform of Manual Injection of Healing System into Crack Plane of a Specimen

2.3 Microencapsulation

As illustrated before, an effective method of delivering the healing agent to the damage site is through encapsulation of the healing agent. The encapsulation of the healing chemistry is an effective way to protect the healing chemistry from deactivation by air, water, and to some degree, high temperature. The healing chemistry is

protected and stored in the capsules and embedded into coating. During the service of the coating, any damage or cracks will rupture the embedded capsules and release the healing chemistry.

The UF encapsulation process is developed by S.R. White et al [15]. The healing agent used in Whites work is dicyclopentadiene (DCPD). In his synthesis process, urea, resorcinol and ammonium chloride are mixed in de-ionized water, then, ethylene maleic anhydride copolymer (EMA) solution was added. After adjusting the pH to 3.5 by using drops of NaOH or HCl, the DCPD and formaldehyde was added into the solution. Finally, the solution was heated to 55 °C and the temperature maintained for four hours. During this time the solution was agitated at a specific rate (from 300 rpm to 600 rpm) resulting in the emulsion polymerization of the urea formaldehyde creating microcapsules. Microcapsules in the range of $60 - 120$ micrometers with DCPD as core material and urea-formaldehyde as shell were synthesized.

During encapsulating, a surfactant is necessary to adjust the surface interactions between the chemicals. The type of surfactant should be varied to encapsulate different core materials. When encapsulating DCPD, which is hydrophobic, into urea-formaldehyde capsules, EMA was needed to stabilize the DCPD droplets and generate DCPD micelles [65]. Ammonium chloride is used as an initiator and provides the required free radicals. The resorcinol acts as reinforcement in the shell wall creating more robust microcapsules. The urea-formaldehyde encapsulation technique was adapted for linseed oil microcapsules, however, in the urea-formaldehyde and linseed oil system, polyvinyl alcohol (PVA) was used as the surfactant instead of the EMA.

Different encapsulation techniques were attempted for different healing chemistries. In addition to the described urea-formaldehyde encapsulation technique, there are four other major encapsulation techniques [1, 16, 17, 19–21, 23–25]. The synthesis mechanism and process of those encapsulation techniques are shown below. A more detailed description of the procedure for creating the microcapsules is included in the Appendix A.

2.3.1 Urea-formaldehyde Microcapsule Synthesis

When synthesizing urea-formaldehyde microcapsules, the formaldehyde will react with urea to form mono-, di-, and trimethylolureas. The ratio of the formed mono-, di-, and trimethylolureas is 9 : 3 : 1 [66]. Following the formation of the methylolureas, the condensation of methylolureas leads to the growth of chains, which form the linear or cross-linked urea-formaldehyde polymer. This process is demonstrated in Figure 2.4.

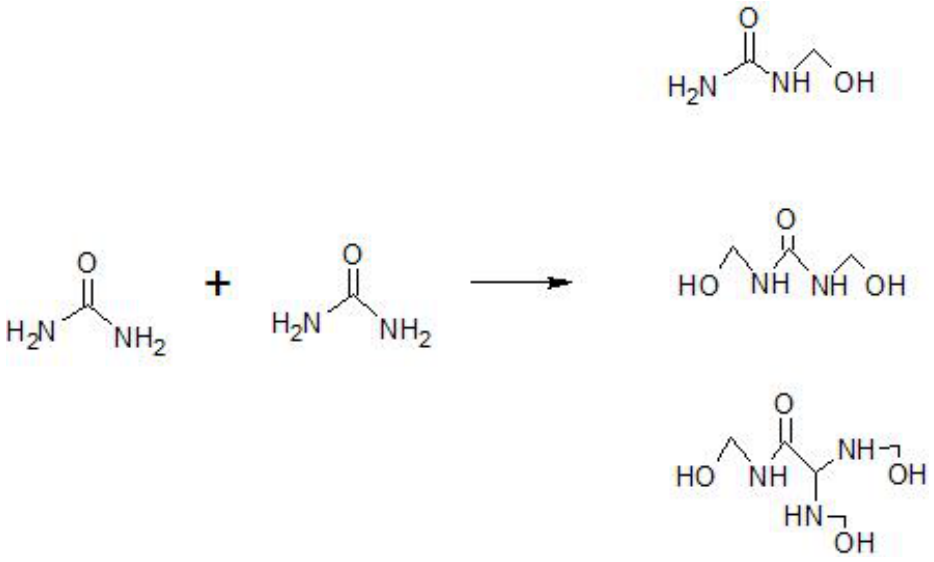

Figure 2.4. The Formation of the Methylolureas

The synthesis process of urea-formaldehyde is presented in Figure 2.6. A detail synthesis receipt can also be found in Appendix B. According to Yuan Li [20], in order to get the highest core content and yield, the best urea and formaldehyde weight ratio is 0.5 to 1.

2.3.2 Phenol-formaldehyde Microcapsule Synthesis

Alternative types of microcapsules are possible and were tested for material compatibility, ease of manufacture, and suitability for use as a healing system. Using

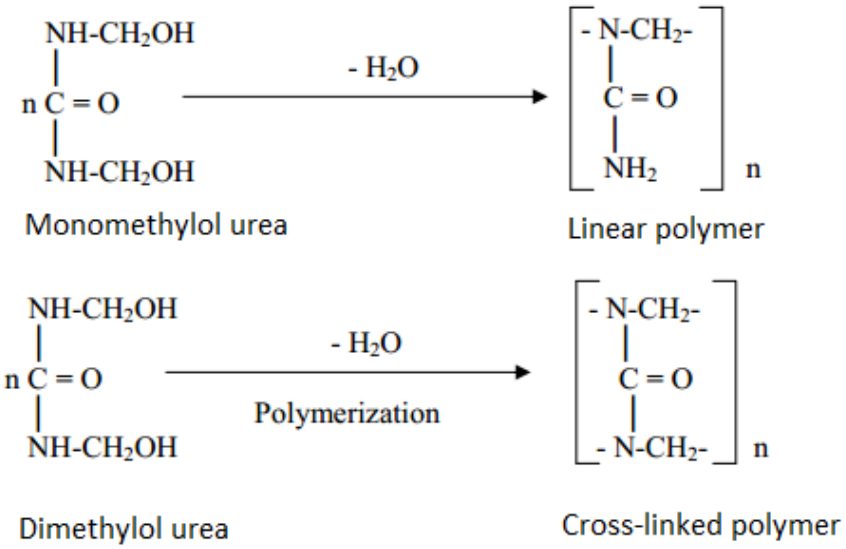

Figure 2.5. Chain Growth of Methylolureas

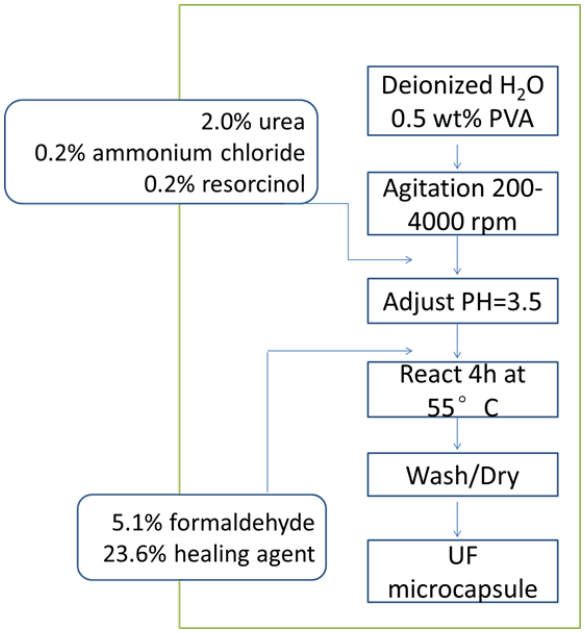

Figure 2.6. The Process of Synthesizing Urea-formaldehyde Microcapsules. From Ref. [65]

Boiled Linseed oil as the core material alternative microcapsule shell materials were evaluated. Phenol-formaldehyde microcapsules, which was first designed by Jadhav in 2010 [24], was used to encapsulate linseed oil. Due to the fact that it was difficult to achieve high yields of filled capsules, the price of phenol is much higher than urea, and phenol also poses greater health hazards phenol-formaldehyde microcapsules were not chosen for the standard self-healing coating.

Using encapsulating linseed oil as an example, the process to synthesis phenol-formaldehyde (PF) microcapsules is given below: 150 ml de-ionized water, 5 ml 5% weight percentage polyvinyl alcohol (PVA). Add 3.76 phenol and 0.5 g ammonium chloride under agitation. Adjust pH to 7 via ammonia. After adding 25 ml healing chemistry, stabilize the solution under agitation for 30 mins. Next, add 6.486g 37% formaldehyde. Stir 2 hr with 250 rpm under 65 °C. Adjust pH back to 3 via 5% weight percentage HCl. Add 0.5g resorcinol. Leave the solution for reaction for 2.5 hr at the same temperature. After filtering, rinse with water and xylene. Similarly, the detail synthesis recipe is introduced in Appendix C. The chemical reaction mechanism is shown in Figure 2.7.

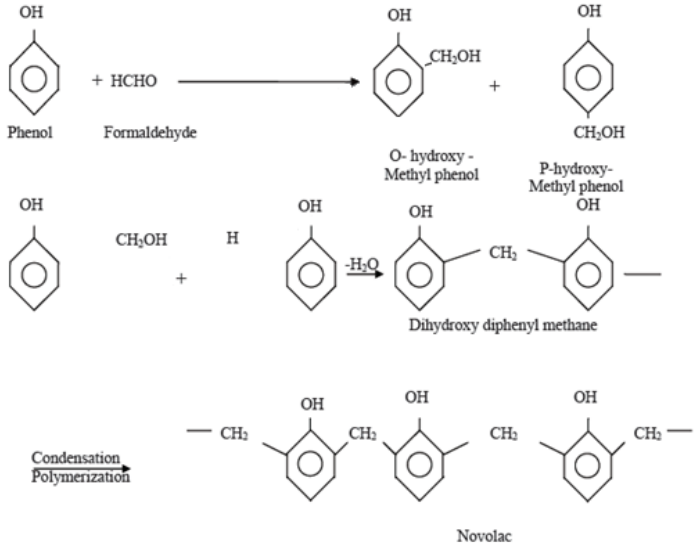

Figure 2.7. The Chemical Reaction of PF Microcapsules. From Ref. [65]

2.3.3 Melamine-urea-formaldehyde Microcapsule Synthesis

Another formaldehyde based microcapsule evaluated is melamine urea-formaldehyde. This encapsulation technique was first reported by Liu [1] in 2009. The advantage of the melamine-urea-formaldehyde (MUF) microcapsule is that MUF microcapsule shell is thicker than urea-formaldehyde shell. The thicker shell can reduce core material leakage during storage. Successful free-flowing, filled microcapsules using melamine-urea-formaldehyde were never achieved after trying this process a number of times.

The melamine urea-formaldehyde microcapsule encapsulation process attempted is provided below: add 3.81 g melamine and 9.55 g formaldehyde into 70 ml deionized water. Allow the solution to react for 25 mins at 70 °C (until everything is dissolved). After getting the MF prepolymer, add 0.84 g urea, 0.5 g ammonium chloride and 0.5 g resorcinol into 200 ml DI water(containing 10 ml 5% wt% PVA). Adjust pH to 3.5. After adding 50 ml healing chemistry and 13 g MF-prepolymer, adjust pH to 3.5 again. Leave the solution for reaction for 4 hr at 55 °C. The detail synthesis process can be found in the Appendix D.

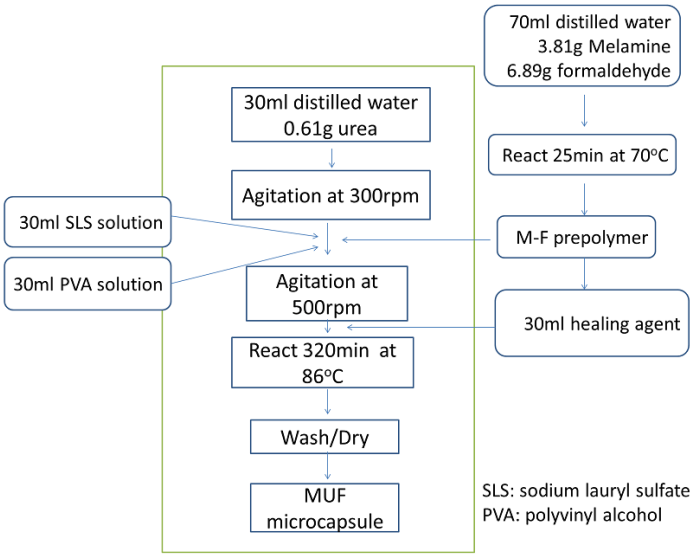

Figure 2.8. The Process of Synthesizing Melamine-urea-formaldehyde (MUF) Microcapsules. [1]

2.3.4 Polyurethane Microcapsule Synthesis

Polyurethane(PU) microcapsules were also evaluated as an alternative encapsulation technique. Polyurethane microcapsules were first introduced by Cho et al [34] when he was developing a more water robust self-healing polymer. PU microcapsules will be a good choice if a urethane coating instead of an epoxy coating is desired. Urethane coatings are popular coatings used in off-shore industries. However, the PU microcapsules synthesis process is much more complex and expensive than urea-formaldehyde microcapsules. Additionally, during the synthesis of polyurethane prepolymer, it was very common to obtain a useless gel instead of the PU prepolymer. The chemical reaction and the PU microcapsule synthesis process are shown in Figure 2.9 and Figure 2.10.

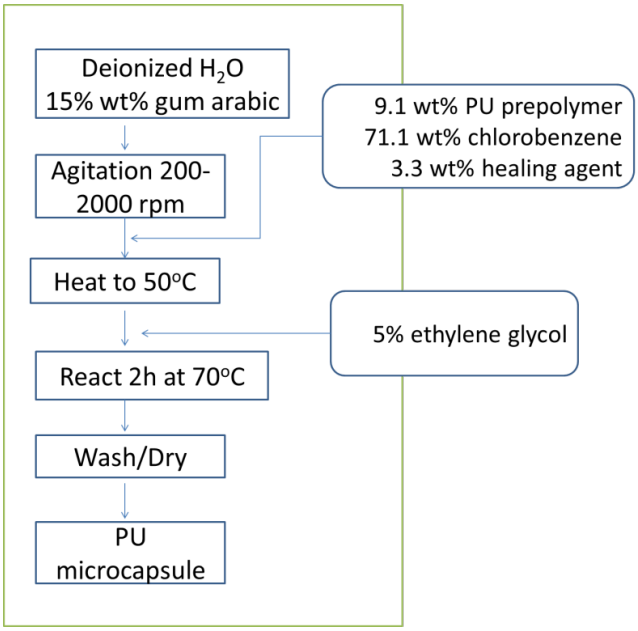

Figure 2.9. The Chemical Reaction during Synthesizing PU microcapsules. [34]

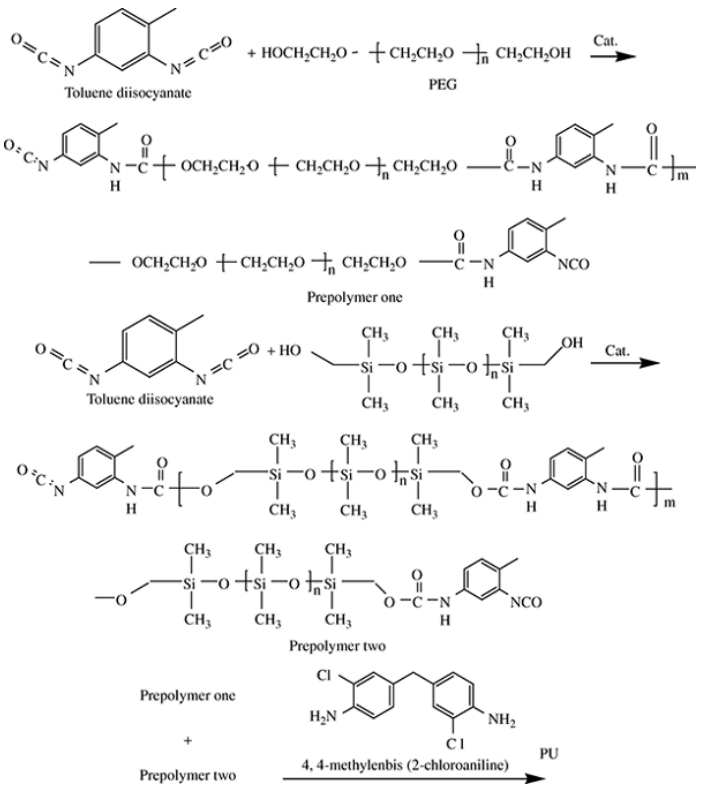

Figure 2.10. The Chemical Reaction during Synthesizing PU Microcapsules. From Ref. [65]

2.4 Mechanical Testing

Mechanical tests were performed on a MTS 810 servohydraulic testing machine. Using a 100 lbf load cell, and a LabVIEW DAQ. All experiments using the material testing system (Figure 2.11) were performed in displacement control.

The functionality of the MTS system can be changed by changing the grips used to hold the specimen. Custom grips for four point bending tests and tensile clamping grips for evaluation modulus are shown in Figure 2.12.

A custom data acquisition system was developed with LabVIEW. LabVIEW is a system-design platform with a visual programming language. The basic four functions of the designed labview program are 1) force and displacement reading 2) force and displacement calibration 3) file initiation and data recording and 4) noise filtering.

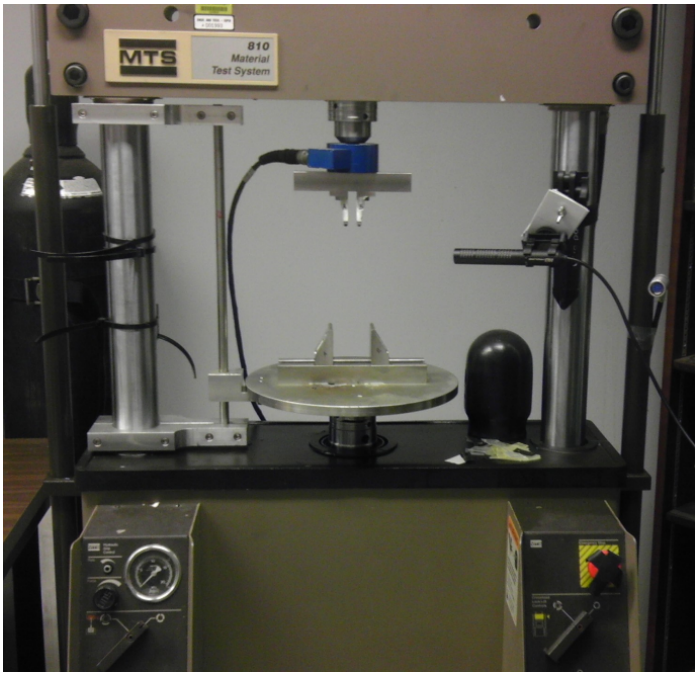

Figure 2.11. Material Testing System (MTS) testing machine

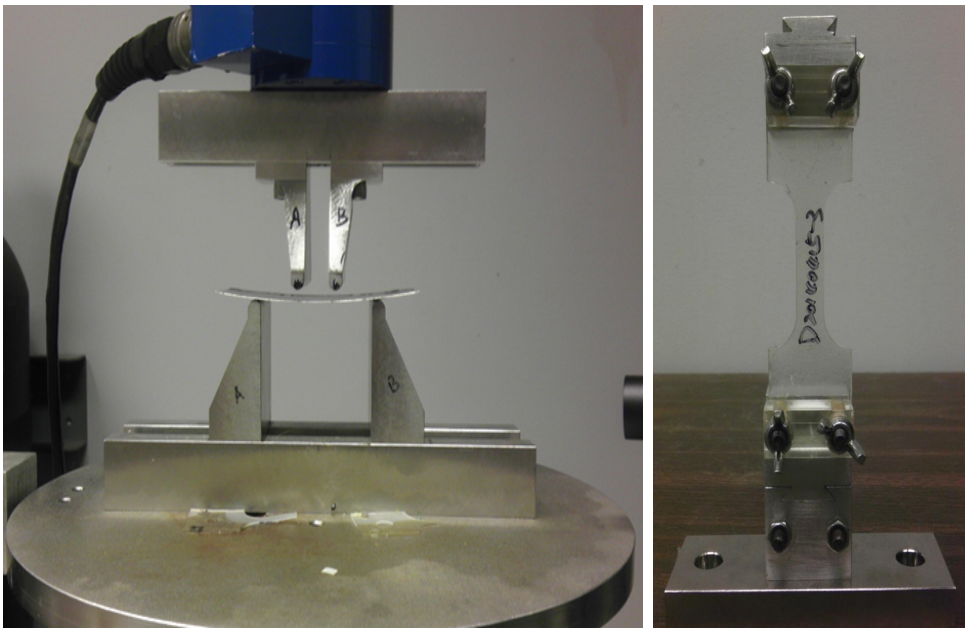

Figure 2.12. Customer Grips for Four Points Flexural Bending Test and Tensile Test

Those functions are achieved through the program design shown from Figure 2.13 to Figure 2.15. The complete circuit of the program is shown in Appendix E.

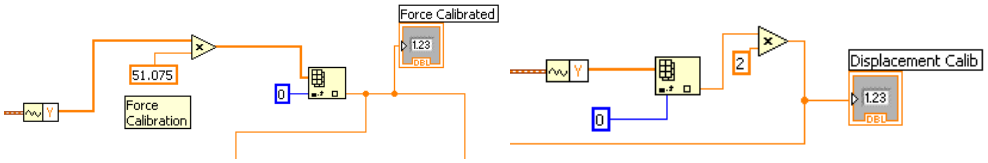

Figure 2.13. Force/Displacement Calibration and Reading Program Circuit

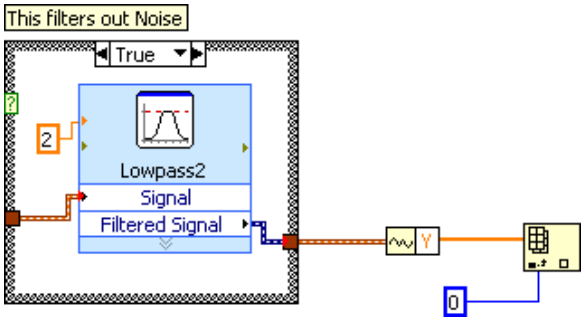

Figure 2.14. Noise Filter Program Circuit

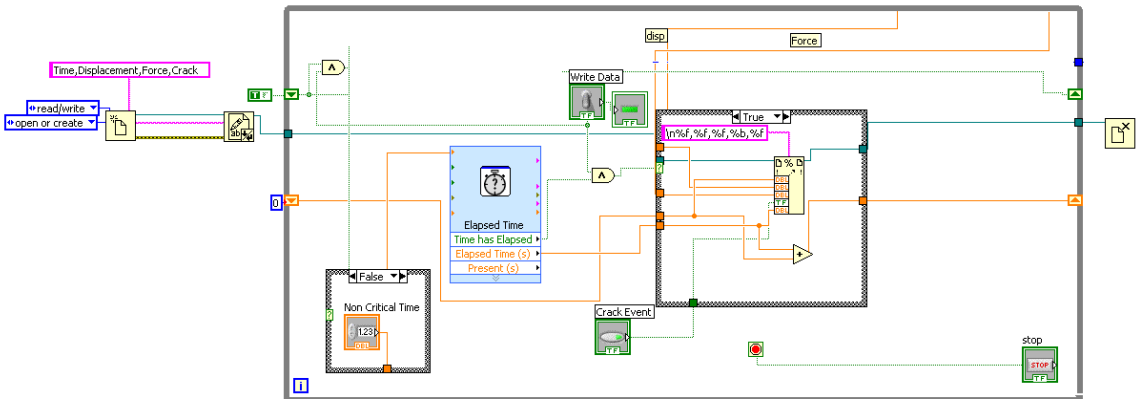

Figure 2.15. Date Recording Program (including file creation, date DAQ and recording frequency control)

A critical component of the custom data acquisition system is an audio signal was used to identify the crack event. A microphone was attached to the frame of the MTS machine and pointed at the specimen to record a crack event. This acoustical detection of cracking is not really possible with conventional data acquisition. A beep sound created by the program (Figure 2.16) and the sound of the initial crack were used together to determine the load at failure due to bending. A beep sound was produced by the LabView program when the system began to record the load data. This sound was detected by microphone and recorded by Sound Recorder. During the loading process, a crack sound produced by the failure of the coating was also detected and recorded. By capturing these two sounds, the time between the beep and crack could be determined by an Adobe Audition, a Audio processing software package. Therefore, the final load at failure could be determined by using the time difference between the initial beep and the crack sound. An example for the process of audio capture and procedure is explain from Figure 2.17 to Figure 2.18.

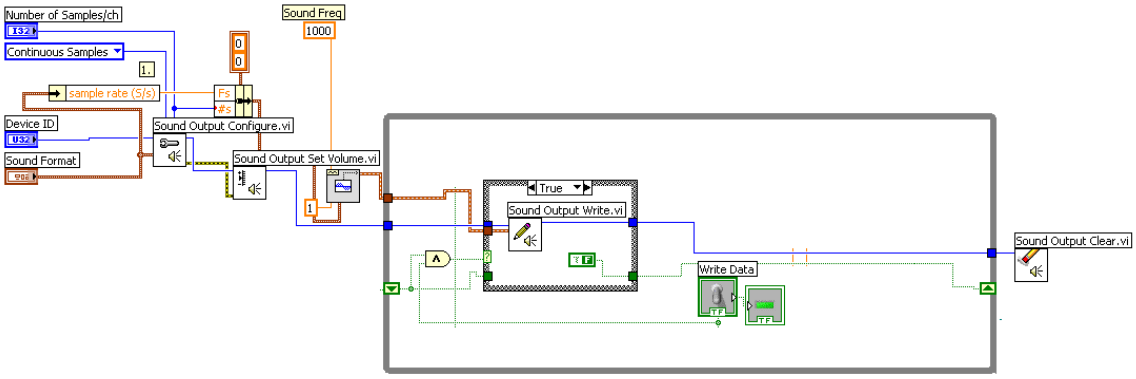

Figure 2.16. Beep Producer Program Circuit

The load that occurred at a time of 16.078s is the load where the specimen cracked.

Another advantage of the LabVIEW is the software provides a clean and visual friendly front platform (shown is Figure 2.19) when running the complex back plat-

Figure 2.17. Sound Recorder Used to Record BEEP and CRACK Sound

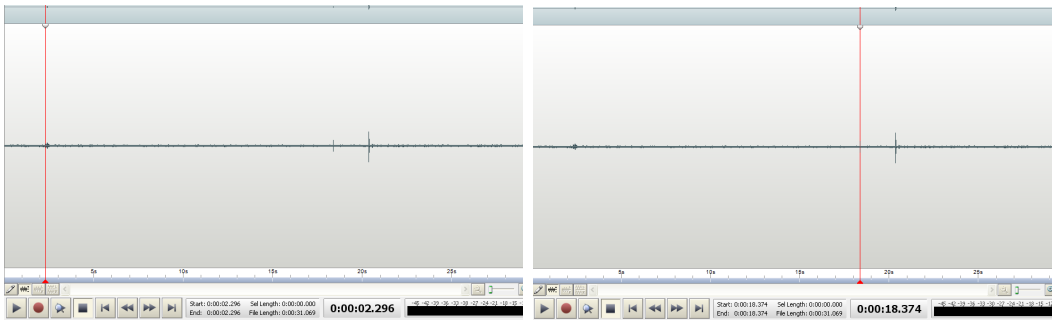

Figure 2.18. The BEEP Sound Was Tracked at 2.296 s; The First CRACK Sound Was Tracked at 18.374 s

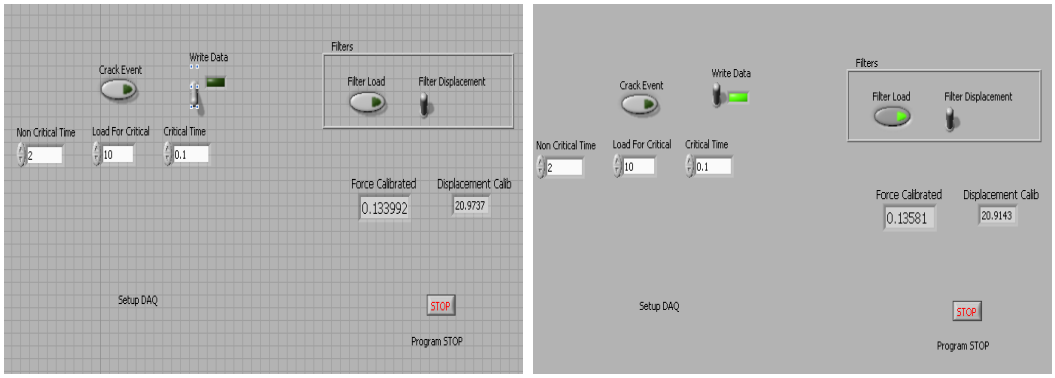

Figure 2.19. The Front Panel of LabVIEW DAQ System Before and After Applying Filter Load and Write Data Function

form program. All controls can be achieved by clicking the controlling items on the front platform.

Test name	ASTM Standards
Modulus testing	ASTM E111-04
Tensile strength testing	ASTM 638

Figure 2.20. ASTM Standards Used for Mechanical Tests

Figure 2.20 exhibits ASTM standards referred when executing mechanical tests.

2.5 Electrochemical Impedance Spectroscopy (EIS)

2.5.1 Equipment and Cable Connection

A Gamry Reference 600 (shown in Figure 2.21) was used to perform Electrochemical Impedance Spectroscopy testing of the coated substrates. Long term corrosion tests were performed by using five PTC1 Paint Testing Cells as shown in Figure 2.22. A 23 flat sample was clamped between a glass tube ($14.6cm^2$) and the Teflon base. The tube is partly filled ($20 - 50$ mL) with the 5 weight percentage NaCl solution, which is the testing electrolyte in the system. A rubber O-ring seal was placed between the sample and glass tube to prevent the leakage of the electrolyte. An Ag/AgCl reference electrode and a graphite rod counter electrode were mounted through a rubber stopper on the top. When doing EIS testing, the flat sample serves as a working electrode and needs to be connected with Green (working electrode) and Blue (working sense) cable on Reference 600. The White cable is the reference cable, which is connected with the Ag/AgCl reference electrode. Red and orange represent counter electrode and counter sense, which are connected with the graphite rod. The Black cable is left open since it is the floating ground. The cell cable connection is exhibited in the Figure 2.24 and 2.23

Figure 2.21. Gamry Reference 600

Figure 2.22. PTC1 Paint Testing Cell and Parts

2.5.2 Parameters Selection

The potentiostate was used for impedance testing of the coated substrate. The impedance tests consisted of applying an alternating current at different frequencies (a frequency sweep) and measuring the effective resistance of the coated substrate. The initial frequency of the frequency sweep was set at $1E + 006$ Hz, and the final frequency was 0.1 Hz. Other parameters selected are shown in Figure 2.25.

Color	Cable Name	Connection
Blue	Working sense	Connect to working electrode-specimen
Green	Working electrode	Connect to working electrode-specimen
White	Reference	Connect to Ag/AgCl reference electrode
Red	Counter electrode	Connect to counter electrode- graphite rod
Orange	Counter sense	Leave open
Black	Floating ground	Leave open

Figure 2.23. The Terminal of the Each Cable

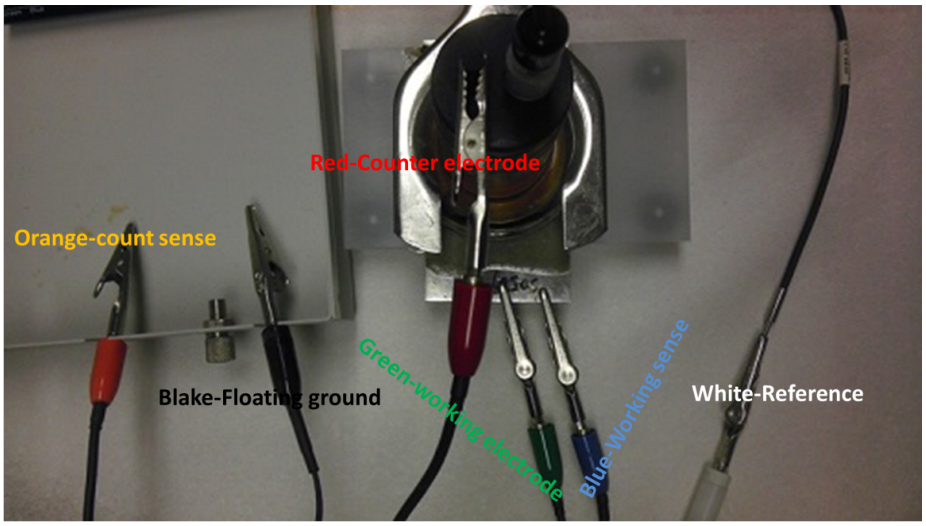

Figure 2.24. The Cable Connection Diagram

A typical result of the impedance test is impedance at different input frequencies. This data can be represented a number of ways, but the Bode plot and Nyquist plot are the common methods. A typical Bode and Nyquist plot from the impedance tests done with the coated substrates are shown in Figure 2.26.

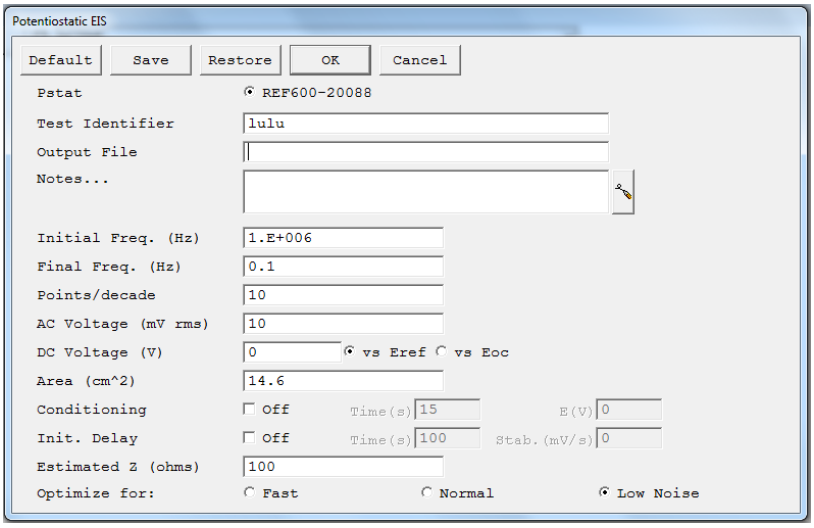

Figure 2.25. Parameter Selection for EIS Test

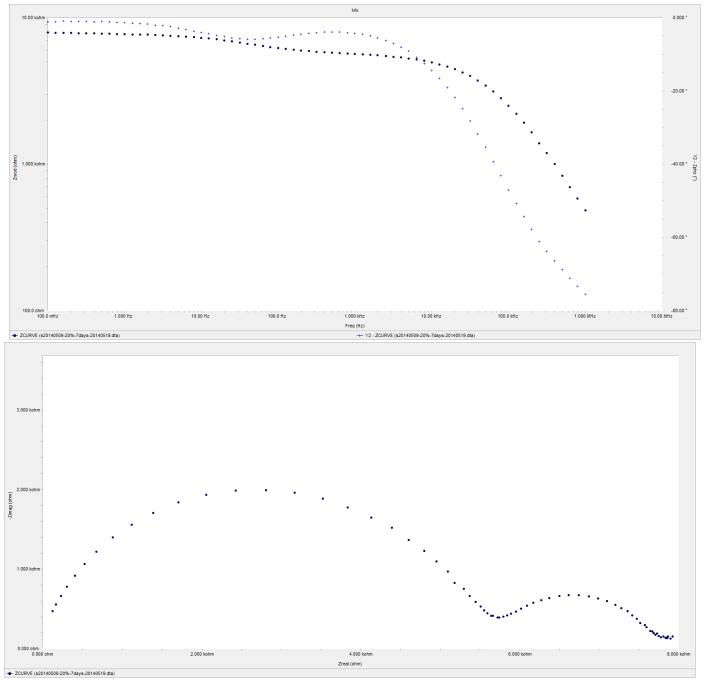

Figure 2.26. A Typical Bode/Nyquist Plot Achieved from Impedance Test

3. DATA ANALYSIS

3.1 Healing Chemistry Selection Result

Seven different possible healing chemistries were evaluated for corrosion prevention performance. A scratch was created by drawing a razor blade across the surface of the epoxy coated specimen. Each specimen consisted of 1074/1075 spring steel coated with 0.5 mm thick epoxy. A typical scratch is shown in Figure 2.3. The healing chemistry under evaluation was compared to a control specimen. The exact procedure was outlined in the experimental section. Electrochemical Impedance Spectroscopy (EIS) tests were also used to evaluate the corrosion protection performance of the healing chemistries. Figure 3.1 shows the corrosion status of the specimens injected with different healing chemistries after 7 days immersion in 5% salt water.

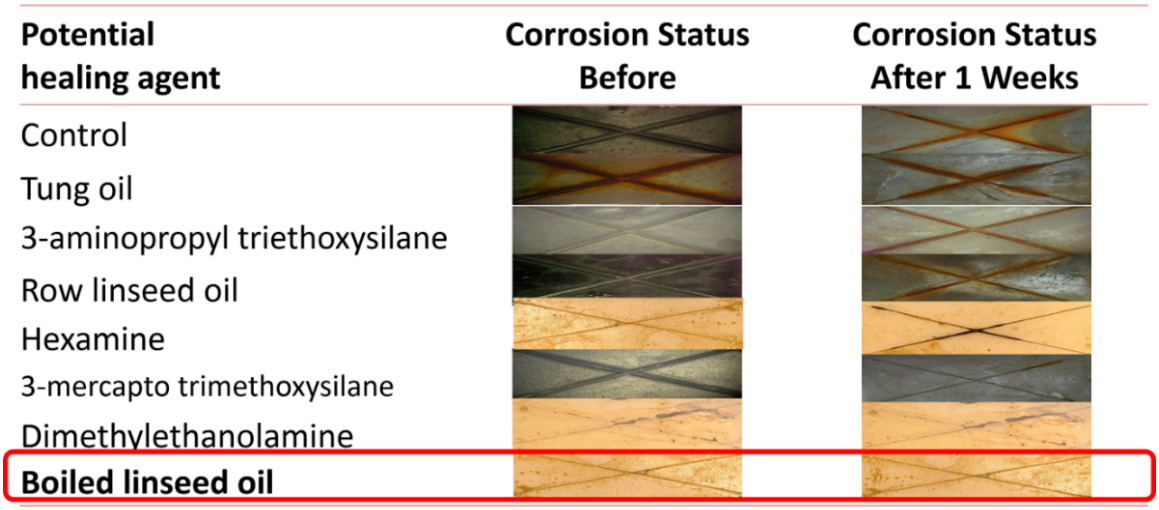

Figure 3.1. Response of Candidate Healing Chemistries

Based on the evaluation of the digital images (as shown in Figure 3.1) the healing chemistries were ranked from best to worst performance. While this method of corrosion protection evaluation does not provide a detailed evaluation of corrosion protection, it does provide an extremely rapid method of evaluating the feasibility of a healing chemistry. The top three healing chemistries were identified as 3-mercapto trimethoxysilane, Dimethylethanolamine and boiled linseed oil and were further evaluated. While focusing on the goal of achieving a low-cost, commercially viable self-healing coating, other considerations included price and safety from a health hazard perspective. The three best performing candidates, 3-mercapto trimethoxysilane, Dimethylethanolamine, boiled linseed oil, along with dicyclopentadiene (DCPD) which is the one of the best structural healing agents, were compared. The comparison results are listed in the 3.2 below. Health hazard data is based on National Fire Protection Association NFPA 704, the standard system for the Identification of the Hazards of Materials for Emergency Response. The four divisions are color-coded. The red division indicates flammability. The blue division indicates level of health hazard, the yellow division is for chemical reactivity, and the white division contains codes for special hazards. Each value of health, flammability and reactivity is rated on a scale from 0 (no hazard) to 4 (severe risk). A complete NFPA diamond example of DCPD is exhibited in Figure 3.1. Here, only the health value is compared. As shown in 3.2, the health hazards of boiled linseed oil is 0, which is much more human and environmentally friendly compared with 3-mercapto trimethoxysilane and dimethylethanolamine, whose health hazards value is 2 and 3 respectively. The price of boiled linseed oil is also competitive since it is used in many other industries and is a naturally occurring renewable product.

As mentioned before, the top three healing chemistries were identified for further evaluation. They are 3-mercapto trimethoxysilane, Dimethylethanolamine and boiled linseed oil. Electrochemical Impedance Spectroscopy (EIS) was used for the ongoing evaluation of the corrosion protection performance among those three healing chemistries. The instrumentation and process for EIS testing can be found in the ex-

Item	Price (per 100ml)	Supplier	Health hazards
3-mercapto trimethoxysilane	$79	Sigma Aldrich	2
Dimethylethanolamine	$112	Sigma Aldrich	3
Boiled linseed oil	$2	Klean Strip	0
DCPD	$21	Sigma Aldrich	1

Figure 3.2. The Comparison Among Healing Agent Candidates [67–70]

Figure 3.3. NFPA diamond of DCPD

periment section. In general, the higher the impedance at a given frequency, the higher the coating resistance (higher resistance indicates better corrosion resistance). Figure 3.4 shows that boiled linseed oil and 3-mercapto trimethoxysilane have significantly better corrosion protection performance over dimethylethanolamine. Additionally, as compared in price and health hazards above, boiled linseed oil and 3-mercapto trimethoxysilane are much more human and environmentally friendly compared to dimethylethanolamine (Figure 3.2). Therefore, boiled linseed oil and 3-mercapto trimethoxysilane were identified as the best candidates for the self-healing coating. Each healing agent was then encapsulated to evaluate the encapsulation process. Different trials to encapsulate boiled linseed oil and 3-mercapto trimethoxysilane are presented in the next section.

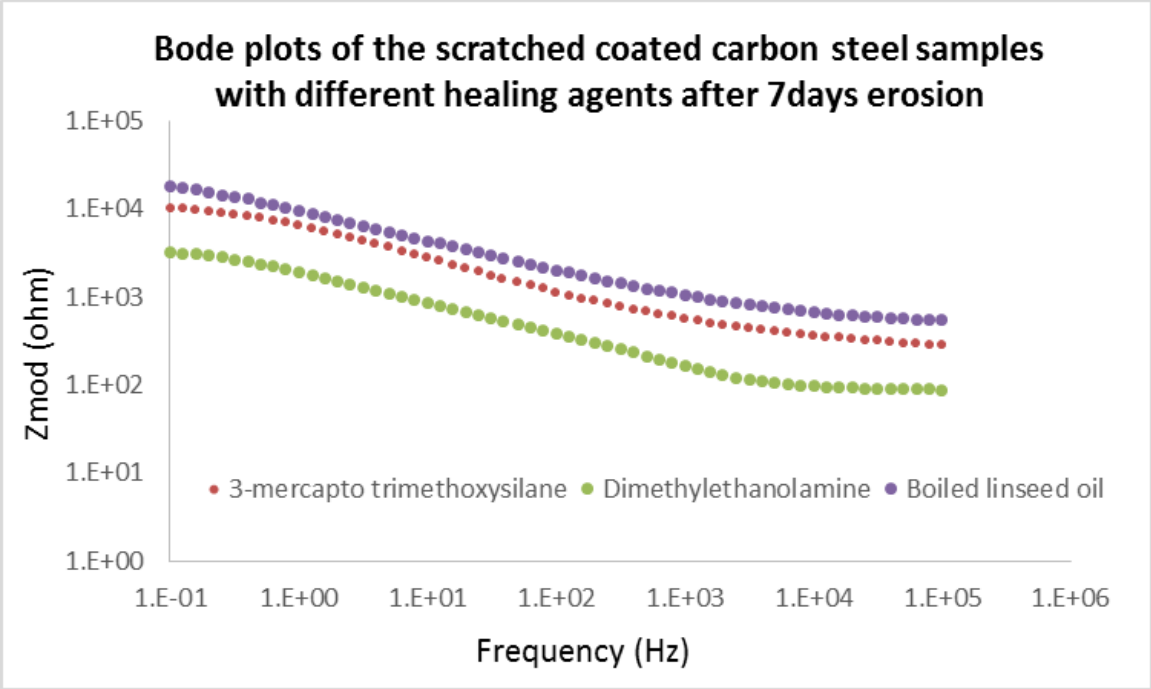

Figure 3.4. Dimethylethanolamine, 3-mercapto trimethoxysilane and Boiled Linseed Oil Healing Efficiency Comparison

3.2 Different Encapsulation Techniques

Both phenol-formaldehyde(PF) and urea-formaldehyde(UF) encapsulation techniques were used with 3-mercapto trimethoxysilane as the core material. The detailed chemical reaction and the synthesis process were presented in the experimental section. However, neither PF nor UF encapsulation techniques created viable microcapsules with the 3-mercapto trimethoxysilane. Numerous parameters during the encapsulation process were varied and in all cases the PF encapsulation technique resulted in viscous, semi-solid similar in consistency to yogurt, while the UF encapsulation technique created empty capsules. Examples of these results are shown in Figure 3.5.

Boiled linseed oil was also evaluated with phenol-formaldehyde encapsulation, melamine urea-formaldehyde encapsulation and urea-formaldehyde encapsulation tech-

niques. The detailed chemical reactions and the synthesis process can also be found in the experimental section. The urea-formaldehyde microcapsules were fully filled with the linseed oil and provided a high success rate of encapsulation. Similarly, although numerous parameters were varied during the encapsulation process of using the PF and MUF encapsulation techniques, no viable microcapsules were produced. Examples of these results are shown in Figure 3.6. Therefore, the urea-formaldehyde encapsulation technique with the boiled linseed oil as core material was identified as the best candidate for the self-healing coating.

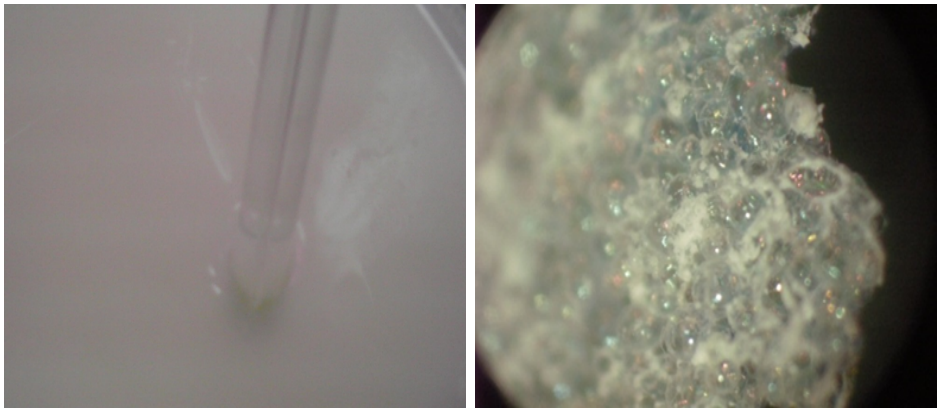

Figure 3.5. Encapsulate 3-mercapto trimethoxyysiane with *a*) Phenol-formaldehyde *b*) Urea-formaldehyde Microcapsule

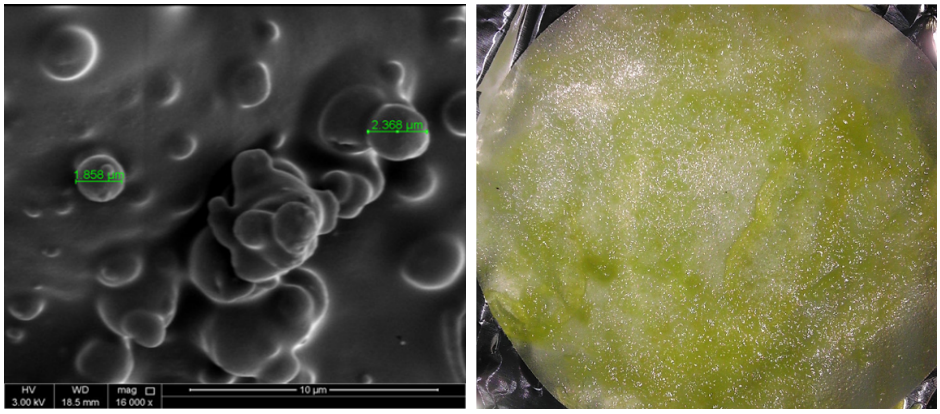

Figure 3.6. Encapsulate Boiled Linseed oil with *a*) Phenol-formaldehyde *b*) Melamine-urea-formaldehyde Microcapsule

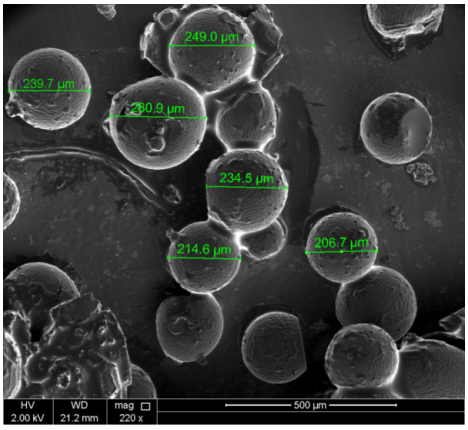

Figure 3.7. Encapsulated Urea-Formaldehyde Microcapsule with Boiled Linseed Oil

3.3 Microcapsule Characterization

After the best candidate for healing agent and microcapsule shell wall were identified, the characterization of the microcapsule system started. All of the following microcapsule characterization, mechanical tests and corrosion resistance tests are all based on boiled linseed oil as healing agent with urea-formaldehyde (UF) as the shell wall. In this section, the impact of stirring speed on the size distribution of capsules, thermal, and storage stability will be discussed.

3.3.1 The Impact of Stirring Speed on the Size of Capsules

Microcapsule Morphology

Microcapsules in Figure 3.8 were synthesized using different stirring speeds. All the capsules are well filled with core material and most obtained the desired round shape. The average diameters of the capsules synthesized under 300 rpm, 400 rpm, 500 rpm and 600 rpm stirring speed are 254μm, 171μm, 162μm and 46μm respectively.

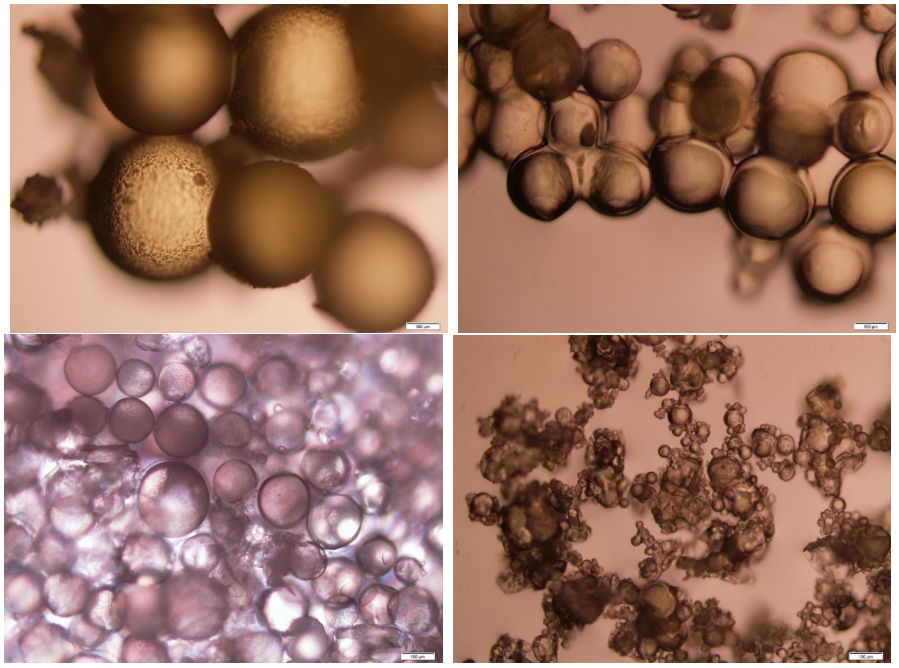

Figure 3.8. Optical Microscopy Pictures of Microcapsules under 300 rpm, 400 rpm, 500 rpm and 600 rpm Stirring Speeds

Microcapsule Size Distribution

There is a distribution of microcapsule sizes at a given stirring speed due to the boundary layers in the agitated solution. Droplets of core material near the stirring blade are broken up creating smaller droplets and therefore smaller microcapsules, on the other hand, droplets near the outside edge of the beaker remain larger. Typical distributions of the microcapsule size given a stirring speed are provided below in Figure 3.9.

The size distribution data is also presented in Figure 3.10. We can see that, capsules synthesized under 400 rpm and 500 rpm stirring speed show similar average diameter. However, with higher stirring speed, the capsules tend to have wider size distribution.

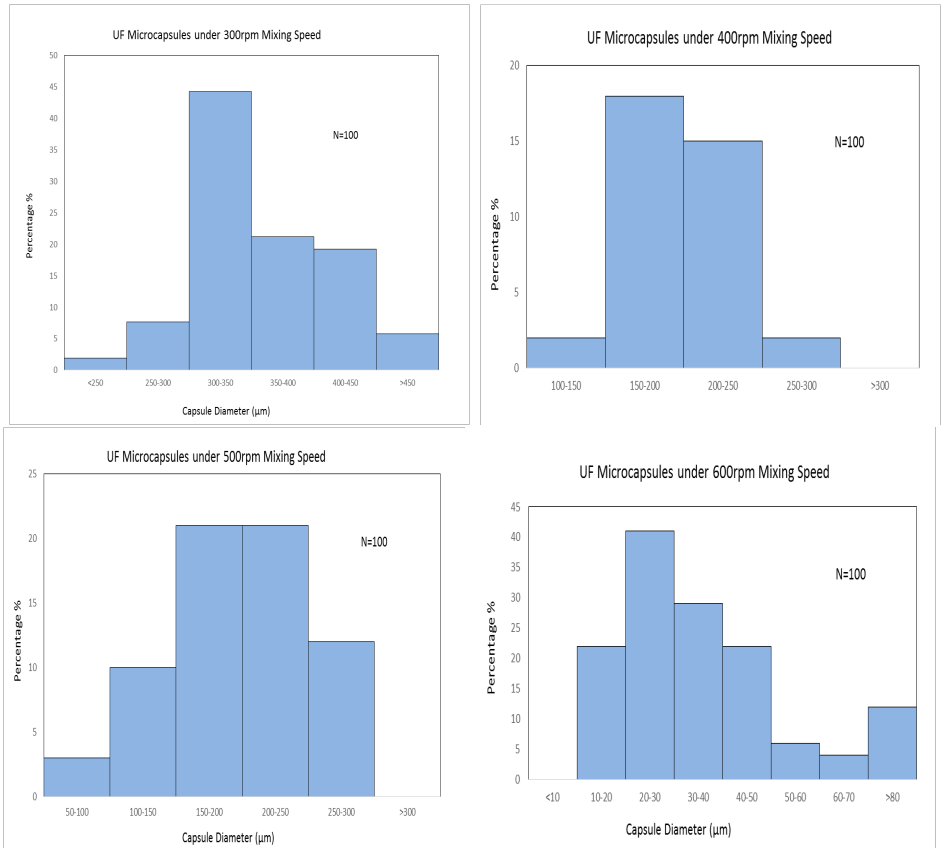

Figure 3.9. Size Distribution of Capsules Made under 300, 400, 500 and 600 rpm Stirring Speeds

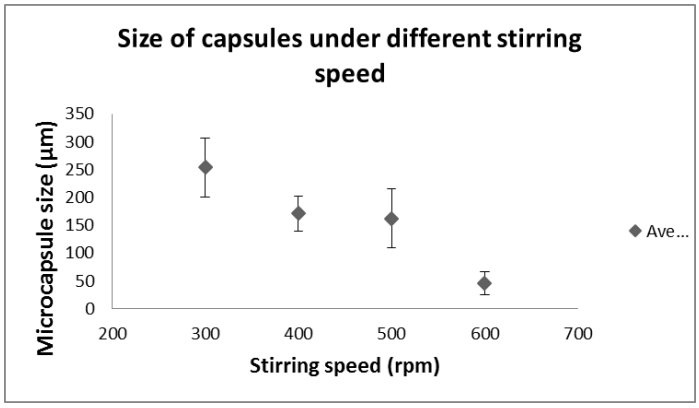

Figure 3.10. Size Distribution of Capsules under Different Stirring Speeds

Stirring speed rpm	Ave. diameter (μm)	STDev (μm)	STDev/Ave. %
300	254	53	21
400	171	32	18
500	162	53	33
600	46	20	45

Figure 3.11. Statistical Distribution of Capsules under Different Stirring Speeds

Shell Thickness of Microcapsules

The Scanning Electron Microscope (SEM) was used to evaluate the shell thickness of the microcapsules. The microcapsules were coated with a layer of gold to increase the conductivity during electron irradiation. Morphology of the synthesized microcapsules are shown in Figure 3.12. The thickness of microcapsules shell ranges from 3μm to 9μm, with an average of 6μm.

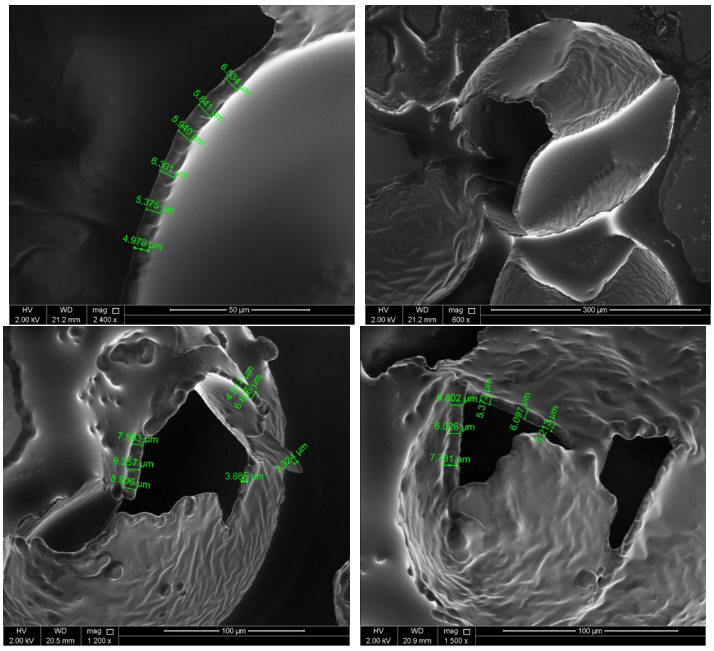

Figure 3.12. Shell Thickness of Capsules Synthesized under 400 rpm Stirring Speed

3.3.2 Thermal Stability and Core Material Content of Capsules

Thermogravimetric analysis (TGA) was used to evaluate the thermal stability of the microcapsules and provide estimates for the relative amount of core material in the microcapsule. The microcapsules were placed in a nitrogen atmosphere and the temperature was increased from room temperature to 600 °C at a 10 °C/min heating rate. Figure 3.13 shows a slow weight loss beginning at 100 °C due to removal of residual water and xylene. The weight loss beginning at 200 °C is due to the decomposition of urea-formaldehyde shell. The weight loss starts near 349 °C, which is the boiling point of linseed oil. In all cases, the microcapsules loose very little weight at temperature below 200 °C. Figure 3.14 shows the relative core content to shell wall content of the microcapsules at different stirring speeds. A number of observations can be made based on this data. Specifically, the core material content of the capsules can reach above 80% for all the capsules and the smaller capsules, which are made using a faster stirring speed, lowers the core material content. This phenomenon agrees with theatrical calculations of the core material content.

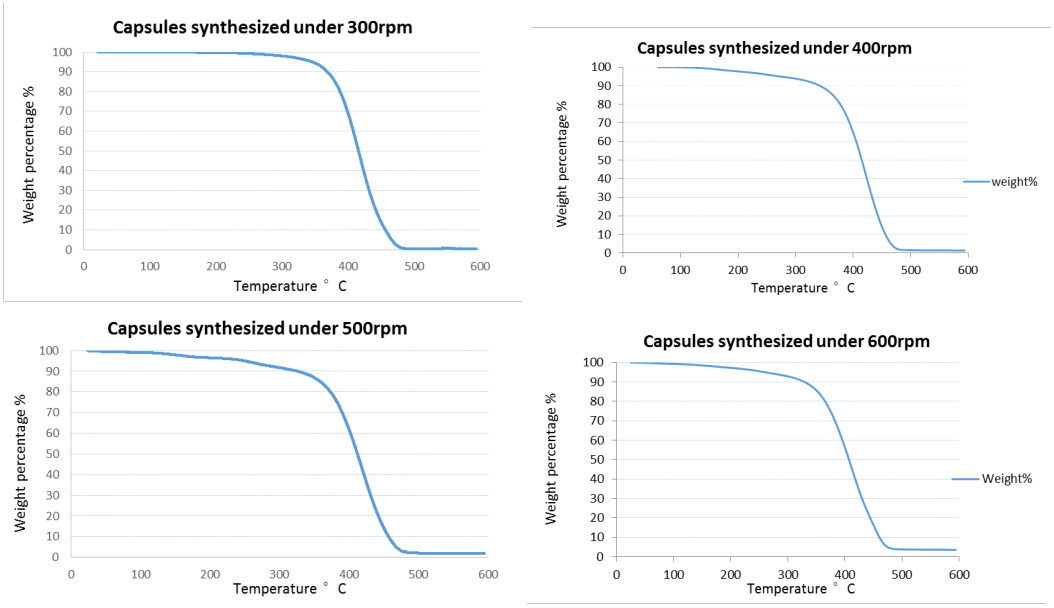

Figure 3.13. Thermogravimetric Analysis(TGA) of Capsules Synthesized under Different Stirring Speeds

Stirring speeds	300rpm	400rpm	500rpm	600rpm
Core material %	94	87	85	82

Figure 3.14. Core Material Content in Capsules under Different Stirring Speeds

3.3.3 Storage Stability of Microcapsules

While the TGA data indicates that the microcapsules should remain relatively stable at room temperature for long time periods, the processing of the microcapsules creates some problems in their long term durability. After fabrication, any linseed oils that was not encapsulated will end up coating the outside of the microcapsules. Xylene was used to remove the remaining linseed oil from the outside of the capsules. Xylene is able to remove the majority of the linseed oil coating the outside of the microcapsules, however, the residual xylene itself will cause the capsules to stick together. This is a problem since the microcapsules will be more difficult to store, weigh, and distribute evenly in the epoxy matrix, in addition the stickiness leads to breaking of the microcapsule shell walls, which will continually cause the capsules to leak. This problem is obvious by the way the microcapsules handle as well as by looking at SEM images of the microcapsules after different storage times. Figure 3.16 shows the microcapsules after three different storage times.

The microcapsules were also evaluated using TGA. After one month of storage, the core material content of 300 rpm capsules decreased to 85.7%. After three months storage, the core material content decreased to below 80%. Compared to the TGA data of the newly synthesized capsules, there is 8% and 14% core material loss after one month and three months storage respectively (Figure 3.17).

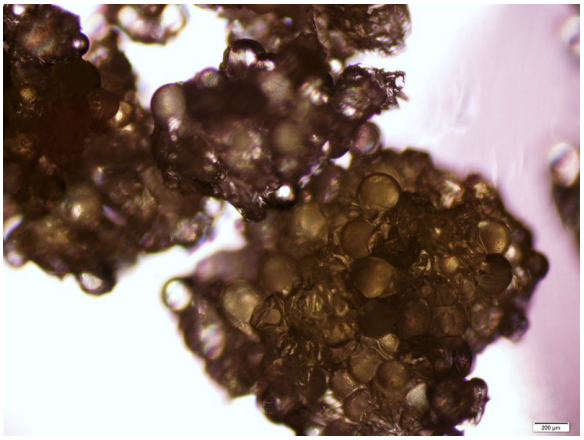

Figure 3.15. Capsules Only Rinsed with Water Shower After 3 months Storage

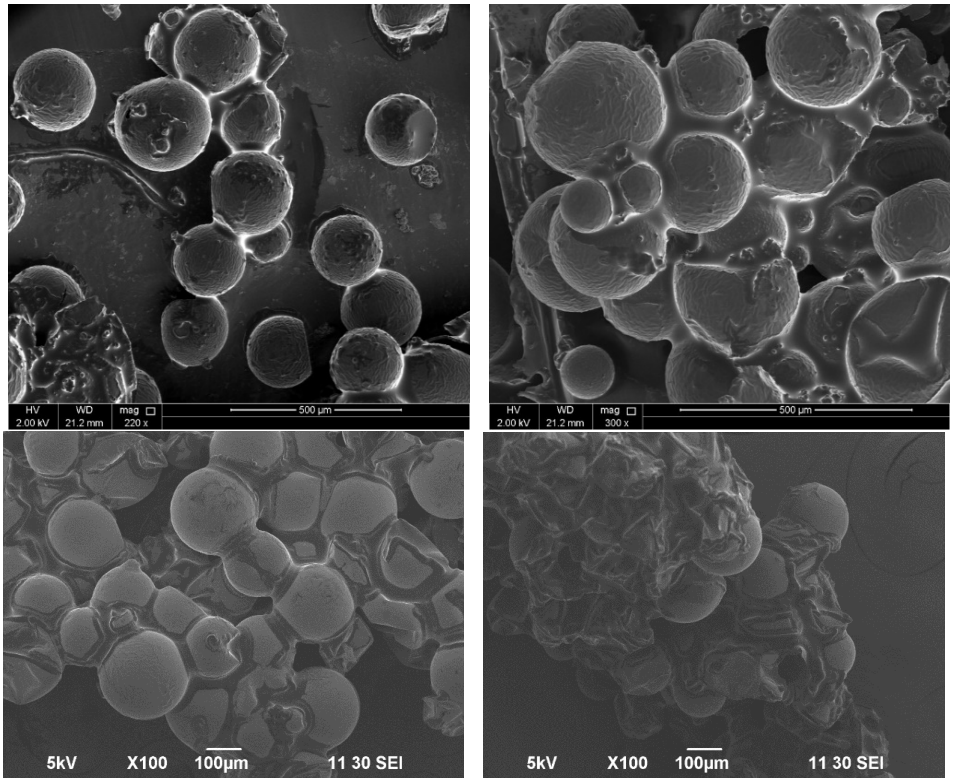

Figure 3.16. SEM Image of Capsules Rinsed with Xylene *a*) Newly Synthesized *b*) After one week Storage *c*) One Months Storage *d*) Three Months Storage

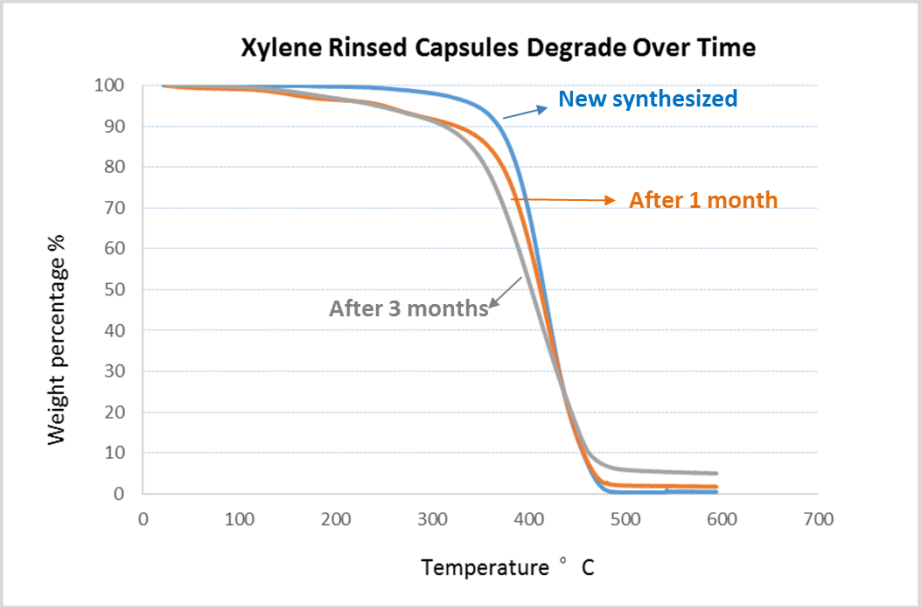

Figure 3.17. Xylene Rinsed Capsules Degrade Over Time

3.4 The Trials to Solve the Stickiness of Microcapsules

3.4.1 The Impact of Rinse-solution on the Capsules Morphology

Figure 3.18 shows microcapsules that were rinsed only with water. This shows that the newly synthesized capsules are sticky together. It is result from the remaining linseed oil around the capsules. Therefore, in lots of literatures [1, 21–26], xylene was used to remove the remaining linseed oil. However, the xylene itself will cause sticking and the continual leakage of the capsules. In order to solve the stickiness of capsules and reduce the damage caused by remaining xylene, different solutions were used to rinse the microcapsules. Ethanol, palmolive soap, a solvent mixture of xylene/water (1:9 ratio by volume), and a 0.1 M/L NaOH solution were all tried. The capsules rinsed by ethanol (shown in Figure 3.19.a) were still surrounded by a residual layer. Infrared Spectroscopy analysis shown that the residual layer was linseed oil. Therefore, ethanol could not remove the remaining linseed oil effectively. Palmolive soap could remove the remaining linseed oil well, however, because of the

existence of soap bubbles, any empty capsules (broken shell pieces or precipitated UF) could not easily be removed from the in-tact microcapsules (Figure 3.19.*b*). The combined mixture of the empty or broken capsules with the in-tact microcapsules was undesirable for use in the coating. The solvent mixture could remove the shell and remaining linseed oil well, but the problem of the remaining xylene could still not be avoided(Figure 3.19.c). Finally, a solution of 0.1M/L NaOH was used to try to remove the linseed oil. Figure 3.19.*d* is the image of capsules rinsed by 0.1 M/L NaOH solution, showing few broken or empty microcapsules.

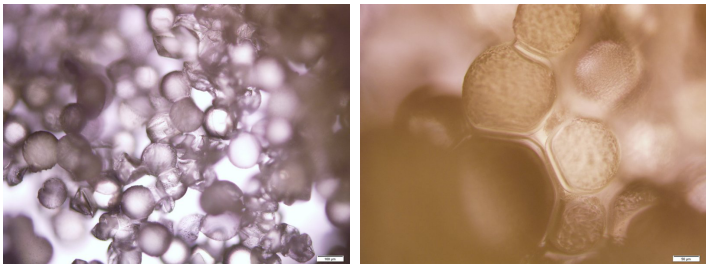

Figure 3.18. Pictures of Newly Synthesized Capsules Only Rinsed with Water under Different Magnifications

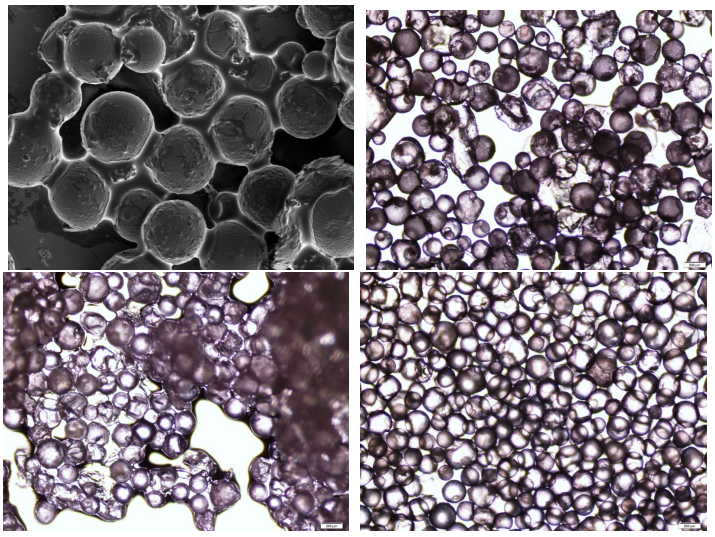

Figure 3.19. Newly Synthesized Capsules Raise with *a*) Ethanol *b*) Soap *c*) Solvent Mixture *d*) 0.1 M/L NaOH Solution

Applying TGA analysis of capsules rinsed by 0.1M/L NaOH solution, after one month of storage, the core material content of capsules which were synthesized under 400 rpm decreased to 84.7%. After three months storage, the core material content decreased to 82.5%. Compared with the TGA data of the newly synthesized capsules, there is only 2% and 5% core material loss after one month and three months storage respectively (Figure 3.20). The thermal stability of capsules rinsed by NaOH shows less core material loss during storage than those rinsed by xylene. It is because NaOH is easier to be removed from the capsules than xylene. Therefore, low density NaOH solution was identified as a better rinsing solvent to remove the remaining linseed oil around the capsules, as well as cause less damage to the capsule shells.

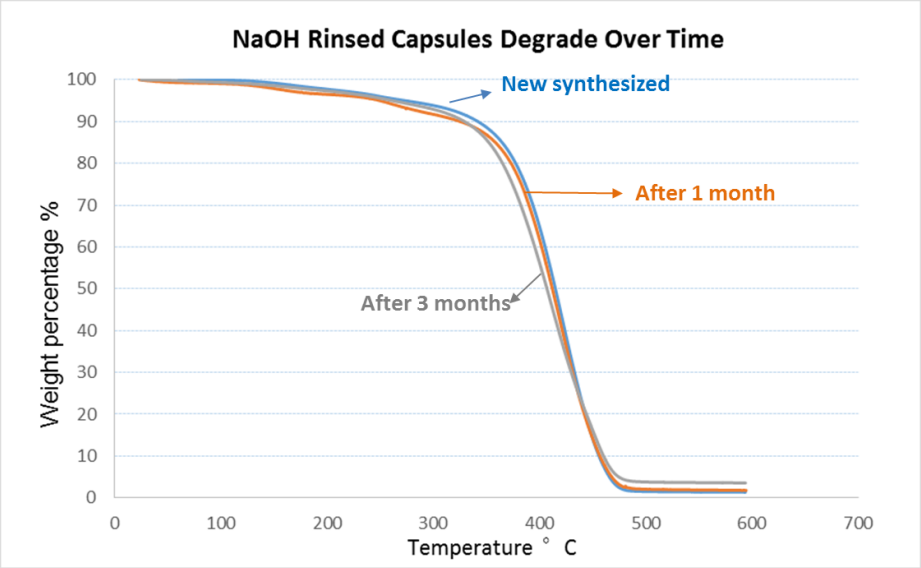

Figure 3.20. NaOH solution rinsed capsules degrade over time

3.4.2 The of Capsules to NaOH Concentration

The concentration of the NaOH solution makes a difference in the final yield of viable microcapsules. A high concentration of NaOH (> 0.2M/L) results in damage and shrinkage of the microcapsules as shown in Figure 3.21. The TGA data in Figure

3.22 also supported that the high concentration of NaOH will break the capsules, especially when the capsules are immersed for long time (48 hr). Strong basic surrounding will force the capsulated linseed oil to release and be consumed. Thats why we see the shrinking capsules in Figure 3.21.

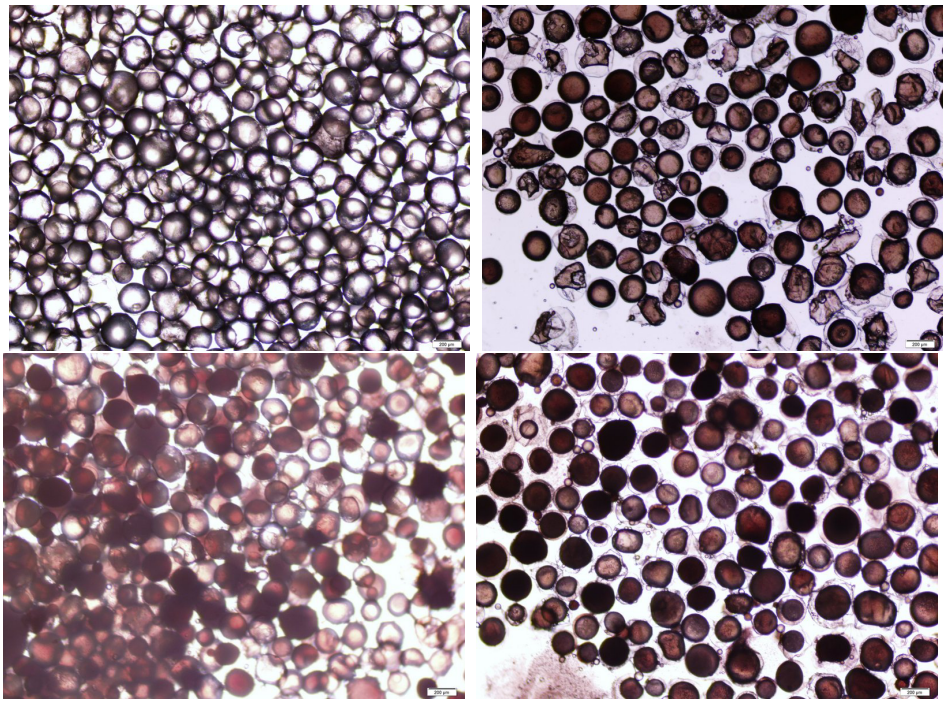

Figure 3.21. Capsules After 12 hr Immersion Into 0.1M/L, 0.2M/L, 0.5M/L and 1M/L NaOH Solution

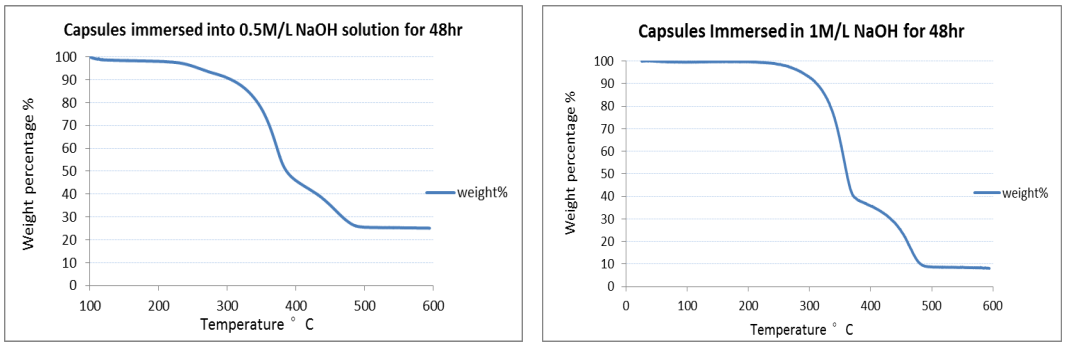

Figure 3.22. Capsules Tolerance to High Density NaOH Solution

3.5 Mechanical Properties of Self-healing Coatings

3.5.1 The Epoxy Coating Embedded With Capsules

Figure 3.23 shows self-healing epoxy coating steel substrates with 5%, 10% 15% and 20% weight percentage of linseed oil, UF microcapsules. The Youngs modulus and bending strength of the coating change depending on the amount and size of the microcapsules. The size of the microcapsules used during this study ranged from 50 to 250 °C.

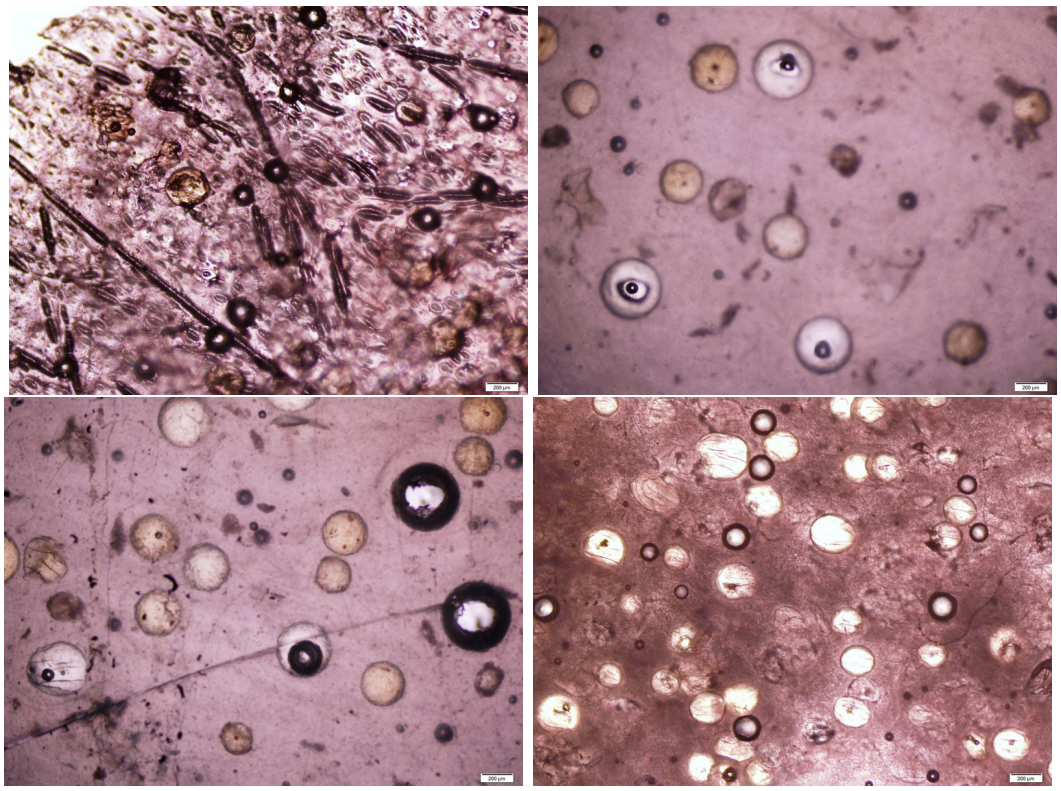

Figure 3.23. Epoxy Coating with 5, 10, 15 and 20 wt% UF-Linseed oil Capsules

3.5.2 Flexural Strength of Self-healing Coatings

Specimens were tested for modulus and bending strength. To calculate the flexural strength of the coating [71] equations (3.1-3.4) were used to calculate the maximum stress in the coating.

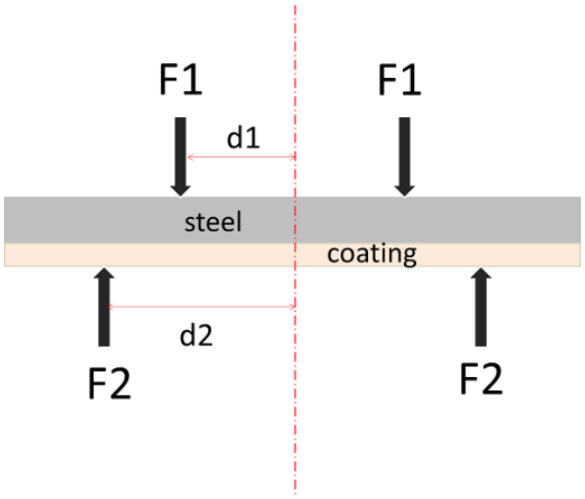

Figure 3.24. Load Condition of the Specimene

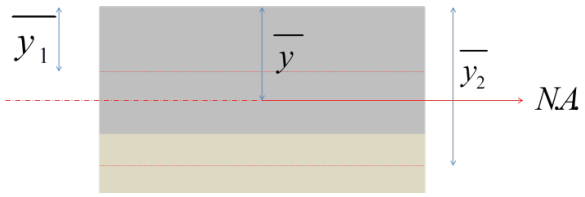

Figure 3.25. Cross Section of the Specimen as A Composite Beam

The neutral axis of the compost beam can be calculated by

$$\bar{y} = \frac{A_1\bar{y_1} + nA_2\bar{y_2}}{A_1 + nA_2} \tag{3.1}$$

$n = \frac{E_2}{E_1}$ is called modular ratio, E_1, E_2 are the Youngs modulus of the coating and steel;

A_1, A_2 are the cross section of the coating and steel;

$\bar{y_1}, bary_2$ are the neutral axis of the coating and steel.

$$I_t = I_1 + nI_2 \tag{3.2}$$

I_t is the moment of inertia of the entire area about the neutral axis.

Therefore, the stress in coating is calculated by

$$\sigma_c = -\frac{nMy}{I_t} \tag{3.3}$$

The maximum moment happens within AB, and the maximum moment is calculated by

$$M = F(d_2 - d_1) \tag{3.4}$$

Figure 3.27 shows the flexural strength of each group of specimen. There are total 17 different groups of specimen (shown in 3.26). Five tests were operated for each group of specimen. The flexural strength data for each group was based on the average value of at least three valid result. As discussed before, the higher stirring speed results in smaller capsules. Here, we found that the smaller the embedded capsules the larger flexural strength of the self-healing coating. When the epoxy coating was embedded with 46 ± 20 μm capsules, which was synthesized under 600 rpm, the flexural strength of self-healing coating can exceed the neat epoxy coating. It is because the UF shell is compatible with epoxy and the bonding between each other is strong enough to withdraw external forces [72]. This phenomenon can also be proved by the increased flexural strength with the increasing of microcapsule weight fracture. However, when the microcapsule weight fracture reach 20%, there is a slight drop of flexural strength. This phenomenon follows the general result of other self-healing coating [72, 73].

Specimen	Capsule size (μm)	Stirring speed (rpm)	Flexural strength (Psi)	Deviation	No. of tests	Observation
Neat epoxy coating			1350	250	15	Coating cracks
Coating with 5% wt%-254 μmcap.	254±53	300rpm	937	180	5	Coating cracks
Coating with 10% wt%-254 μmcap	254±53	300rpm	1006	175	5	Coating cracks
Coating with 15% wt%-254 μmcap	254±53	300rpm	1052	197	5	Coating cracks
Coating with 20% wt%-254 μmcap	254±53	300rpm	995	165	5	Coating cracks
Coating with 5% wt%-171 μmcap.	171±32	400rpm	1146	203	5	Coating cracks
Coating with 10% wt%-171 μmcap.	171±32	400rpm	1200	186	5	Coating cracks
Coating with 15% wt%-171 μmcap.	171±32	400rpm	1317	214	5	Coating cracks
Coating with 20% wt%-171 μmcap.	171±32	400rpm	1251	208	5	Coating cracks
Coating with 5% wt%-162 μmcap.	162±53	500rpm	1278	198	5	Coating cracks
Coating with 10% wt%-162 μmcap.	162±53	500rpm	1251	150	5	Coating cracks
Coating with 15% wt%-162 μmcap.	162±53	500rpm	1211	175	5	Coating cracks
Coating with 20% wt%-162 μmcap.	162±53	500rpm	1276	197	5	Coating cracks
Coating with 5% wt%-46 μmcap.	46±20	600rpm	1478	240	5	Coating cracks
Coating with 10% wt%-46 μmcap.	46±20	600rpm	1451	277	5	Coating cracks
Coating with 15% wt%-46 μmcap.	46±20	600rpm	1476	210	5	Coating cracks
Coating with 20% wt%-46 μmcap.	46±20	600rpm	1392	199	5	Coating cracks

Figure 3.26. ASTM Standard 638 Flexural Strength Results for Bending Test

3.6 Corrosion Resistance of Self-healing Coatings

Before analyzing EIS test results, it is helpful to view an example of the damage and the broken capsules in the epoxy coating. Figure 3.28.a shows the damage site

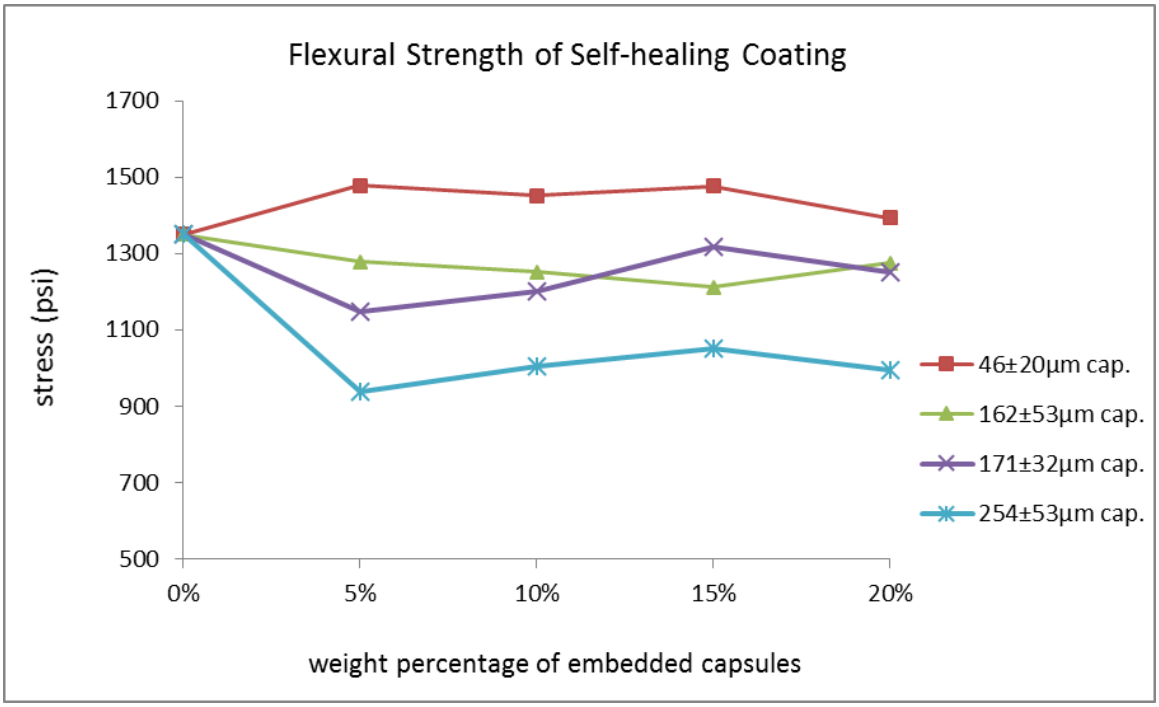

Figure 3.27. The Influence of the Capsule Size and Content to the Flexural Strength of Epoxy Coating

in a coated substrate. The crack was created by drawing a razor blade in a straight line across the specimen. From Figure 3.28.*b*, we see that the crack went through two capsules. Going along the crack, we found there is a liquid with a different color at the intersection of the crack and the broken capsule.

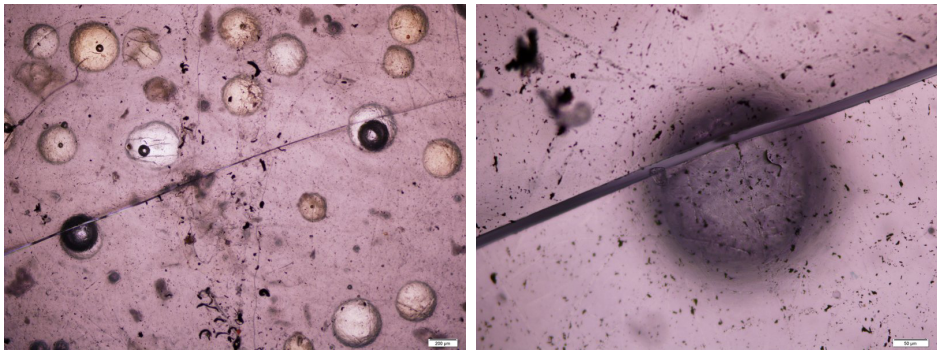

Figure 3.28. Self-healing Process of the Fabricated Self-healing Epoxy Coating

The corrosion protection performance will depend on the number of microcapsules the crack ruptures as well as the size of those microcapsules. While a full study using a statistically valid number of specimens is warranted for this work, the time required to fabricate the self-healing coating components, the number of specimens involved and the long-term testing would be significant and the number of simultaneous testing stations currently available does not make that type of experiment viable for this Thesis. Therefore, the corrosion protection results shown here are illustrative results, performed on a reasonable number of specimens to demonstrate the process for performing these types of tests and the type of conclusions expected from these tests.

The self-healing coating with boiled linseed oil as the core material and urea-formaldehyde as the shell has the significant healing effect compared with control samples. In order to study the mechanism of the healing procedure, an equivalent model for the electrical network for electrochemical impedance spectroscopy of a coated metal surface is needed. The model chosen here is shown in Figure 3.29. The system is composed of five different components. Ru is solution resistance, which represents the electrolyte resistance between the reference electrode and the working electrode. Rpo is Pore resistance. It is the ion conducting paths developed in the coating (it can be regarded as the physical pores on the coating filled with NaCl solution, which gives access for ion conduction). The rust on steel will influence low frequency impedance of the pore resistance. Cc is coating capacitance which could be influenced by water uptake between coating and steel surface. Rf is polarization resistance. The produce of polarization resistance is the potential difference between the actual potential of an electrode and its value at open-circuit. This difference is referred as polarizing the electrode. This process will cause current and the electrochemical reaction at the surface of the electrodes. By evaluating this generated current, we can get the corrosion rate of the system. Cf is Pseudo double layer, which was formed at the interface between the electrode and the electrolyte. The Pseudo double layer acts as a capacitor as shown in the Figure 3.29.

The chronological comparison of each component between the self-healing coating and the control specimen (neat) coating are presented in Figure 3.30 to Figure 3.34. There is no significant difference of Pseudo double layer and polarization resistance between self-healing coating and the control coating. The slight difference of the solution resistance between the self-healing coating and neat coating can be seen in Figure 3.34. This is due to the linseed oil released from the broken capsules will enter the electrolyte and the linseed oil will change the conductivity of the electrolyte. There is a significant difference between the self-healing coating and neat coatings pore resistance, shown in Figure 3.30. The dramatic increase of pore resistance in self-healing coating indicates that the released linseed oil will block the ion conducting path development, needed for the substrate corrosion, in the crack area of the coating. On the other side, the releasing boiled linseed oil reduced the corrosion rate, which reduced the corrosion production accumulation. The corrosion production accumulation will induce coating defects and reducing pore resistance. Figure 3.35 shows that the larger the embedded capsule, the large pore resistance of the self-healing coating.

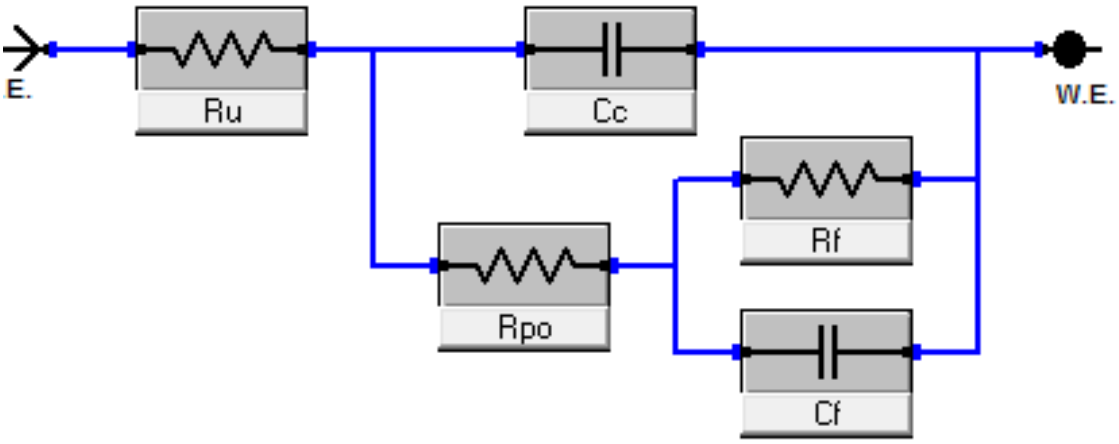

Figure 3.29. Electrical Network Analog for Electrochemical Impedance Spectroscopy of a Coated Metal Surface

Rpo ohms		
Corrosion time	neat coating	Self-healing coating
0hr	2.336	1193
2hr	0.967	1361
6hr	0.838	1637
24hr	0.3648	2059
48hr	0.4576	2562
1week	0.1405	4952

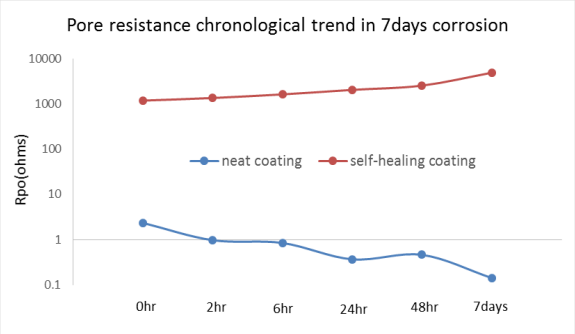

Figure 3.30. The Chronological Trend of Pore Resistance of the Neat/Self-healing Coating in 7 days Immersion

Rf ohms		
Corrosion time	neat coating	Self-healin coating
2hr	0.952	495.9
6hr	0.6513	679.5
24hr	0.5251	1045
48hr	0.4832	1434
1week	1.118	2352

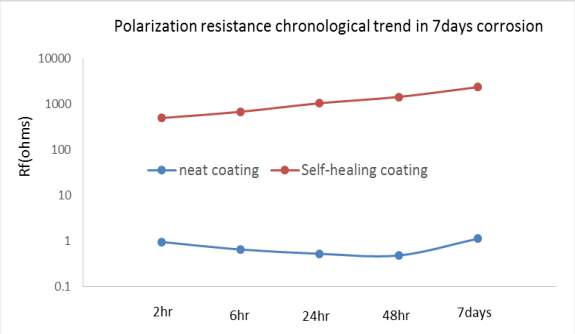

Figure 3.31. The Chronological Trend of Polarization Resistance of the Neat/Self-healing Coating in 7 days Immersion

Cc μF		
Corrosion time	neat coating	Self-healing coating
0hr	8.72E+01	3.32E-04
2hr	5.58E+02	4.35E-04
6hr	1.21E+03	4.58E-04
24hr	4.87E+03	4.90E-04
48hr	1.05E+03	4.73E-04
1week	3.63E+03	4.67E-04

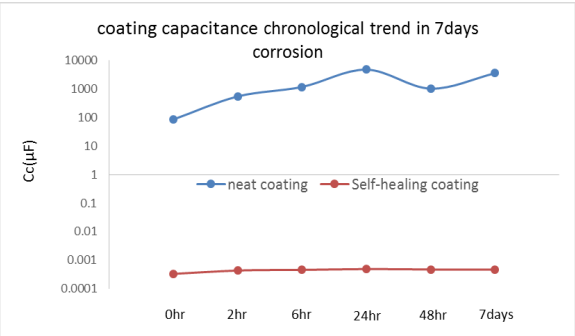

Figure 3.32. The Chronological Trend of Coating Capacitance of the Neat/Self-healing Coating in 7 days Immersion

Cf μF		
Corrosion time	neat coating	Self-healing coating
2hr	1590	4.596
6hr	4461	2.644
24hr	82650	1.35E+00
48hr	48730	1.052
1week	24500	0.8399

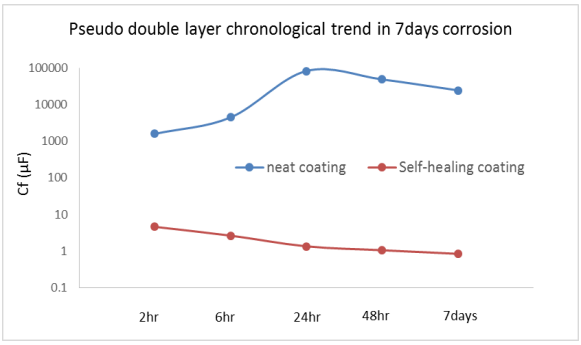

Figure 3.33. The Chronological Trend of Pseudo Double Layer of the Neat/Self-healing Coating in 7 days Immersion

Ru ohms		
Corrosion time	neat coating	Self-healing coating
0hr	24	119
2hr	16	140
6hr	14	152
24hr	10	141
48hr	9	152
1week	18	164

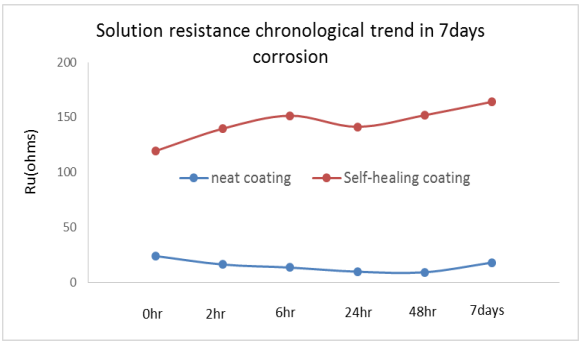

Figure 3.34. The Chronological Trend of Solution Resistance of the Neat/Self-healing Coating in 7 days Immersion

Each component of the equivalent circuit can be evaluated independently, but an overall picture of the performance of the self-healing coating can be seen by investigating the overall impedance performance of the coating. Figure 3.36 shows the impedance of the self-healing epoxy coating with different microcapsule sizes, showing that in general larger microcapsules results in better corrosion protection. This result aligns with the pore resistance comparison among different self-healing coatings. Figure 3.36 also shows how a typical self-healing coating performs versus a control (neat) coated specimen after being submersed in 5% salt water for seven days. As expected, after seven days the self-healing specimen still has significant corrosion resistance, while the neat specimen has no real resistance.

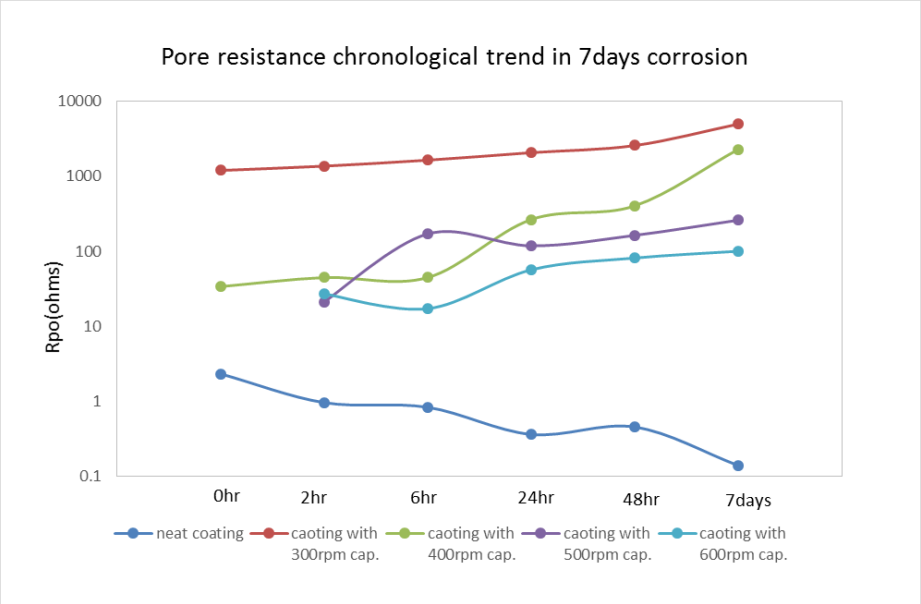

Figure 3.35. Chronological Trend of Pore Resistance of the Neat/Self-healing Coating in 7 days Immersion

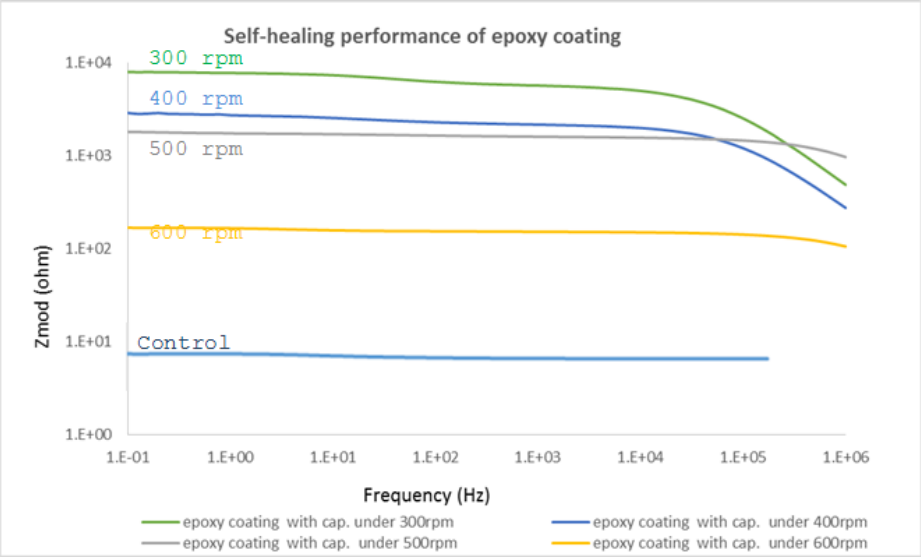

Figure 3.36. Best Corrosion Resistance Performance of Epoxy Coating Embedded with Different Size Capsules. The Weight Percentages of Embedded Vapsules for Sbove Voatings (from large to small) are 20%, 15%, 15%, 20% Respectively

4. CONCLUSION

Seven potential healing agents were evaluated and boiled linseed oil was identified as the candidate healing agent. Different encapsulation techniques were evaluated and urea-formaldehyde microcapsules were chosen as the candidate encapsulation technique. The developed low-cost self-healing coatings with urea-formaldehyde microcapsule and boiled linseed oil as core material satisfies both healing and mechanical properties.

I. The self-healing epoxy coating embedded with UF microcapsules with boiled linseed oil was developed. TGA analysis shown the high content of core material of microcapsule (from 82% to 94%). Significant healing performance of the coating was supported by EIS analysis.

II. The relationship between the stirring speed and microcapsule size distribution was studies. The average diameter of microcapsules was in the range of 46 μm and 254 μm depending on the stirring speed during synthesis. The higher stirring speed produces smaller capsules.

III. 0.1M/L NaOH solution was recommended to remove the residual linseed oil. Microcapsules rinsed by NaOH solution exhibited better thermal stability during storage than those rinsed by xylene.

IV. Epoxy coating fabricated using $46 \pm 20\mu$m microcapsules showed the highest flexural strength while the corrosion protection performance was limited. The coating fabricated using $254 \pm 53\mu$m microcapsules presented the best healing ability while worst flexural strength. Epoxy coating embedded with $171 \pm 32\mu$m microcapsules showed both acceptable healing ability and flexural strength. Therefore, the epoxy coating embedded with 15 weight percentage capsules with $171 \pm 32\mu$m average size is the recommended one.

LIST OF REFERENCES

LIST OF REFERENCES

[1] X. Liu, X. Sheng, J.K. Lee, and M.R. Kessler. Synthesis and characterization of melamine-urea- formaldehyde microcapsules containing enb-based self-healing agents. *Macromolecular Materials and Engineering*, 2009.

[2] F.H.W.A. Corrosion costs and preventive strategies in the united states. Technical report, NACE, 2001.

[3] J.R. Davis. *Corrosion : Understanding the Basics*. ASM International, 2000.

[4] D.A. Jones. *Principles and Prevention of Corrosion*. Prentice Hall, 1995.

[5] W.J. Van Ooij, D. Zhu, and M. Stacy. Corrosion protection properties of organofunctional silanes–an overview. *Tsinghua Science & Technology*, 2005.

[6] V. Palanivel, Y. Huang, and W.J. van Ooij. Effects of addition of corrosion inhibitors to silane films on the performance of aa2024-t3 in a 0.5 m nacl solution. *Progress in Organic Coatings*, 2005.

[7] M.F. Montemor and M.G.S. Ferreira. Cerium salt activated nanoparticles as fillers for silane films: Evaluation of the corrosion inhibition performance on galvanised steel substrates. *Electrochimica Acta*, 2007.

[8] G. Gunasekaran and L.R. Chauhan. Eco friendly inhibitor for corrosion inhibition of mild steel in phosphoric acid medium. *Electrochimica Acta*, 2004.

[9] I. Ahamad and M.A. Quraishi. Bis (benzimidazol-2-yl) disulphide: An efficient water soluble inhibitor for corrosion of mild steel in acid media. *Corrosion Science*, 2009.

[10] B.J. Blaiszik and S.L.B. Kramer. Self-healing polymers and composites. *Annual Review of Materials Research*, 2010.

[11] E.B. Murphy and E. Bolanos. Synthesis and characterization of a single-component thermally remendable polymer network: Staudinger and stille revisited. *Macromolecules*, 2008.

[12] R.J. Varley and S. van der Zwaag. Towards an understanding of thermally activated self-healing of an ionomer system during ballistic penetration. *Acta Materialia*, 2008.

[13] T.A. Plaisted and S. Nemat-Nasser. Quantitative evaluation of fracture, healing and rehealing of a reversibly cross-linked polymer. *Acta Materialia*, 2007.

[14] X.X. Chen, F. Wudl, A.K. Mal, H.B. Shen, and S.R. Nutt. New thermally remendable highly cross-linked polymeric materials. *Macromolecules*, 2003.

[15] S. R. White and N. R. Sottos. Autonomic healing of polymer composites. *Nature*, 2001.

[16] E.N. Brown, M.R. Kessler, N.R. Sottos, and S.R. White. In situ poly(urea-formaldehyde) microencapsula- tion of dicyclopentadiene. *Journal of Microencapsulation*, 2003.

[17] B.J. Blaiszik, N.R. Sottos, and S.R. White. Nanocapsules for self-healing materials. *Composites Science and Technology*, 2008.

[18] B.J. Blaiszik, M.M. Caruso, D.A. McIlroy, J.S. Moore, S.R. White, and N.R. Sottos. Microcapsules filled with reactive solutions for self-healing materials. *Polymer*, 2009.

[19] M.W. Keller, S.R. White, and N.R. Sottos. A self-healing poly(dimethyl siloxane) elastomer. *Advanced Functional Materials*, 2009.

[20] L. Yuan, G.Z. Liang, J.Q. Xie, L. Li, and J. Guo. Preparation and characterization of poly(urea- formaldehyde) microcapsules flled with epoxy resins. *Polymer*, 2006.

[21] S. Cosco, V. Ambrogi, P. Musto, and C. Carfagna. Properties of poly(urea-formaldheyde) microcapsules containing an epoxy resin. *Journal of Applied Polymer Science*, 2007.

[22] Y.C. Yuan, M.Z. Rong, and M.Q. Zhang. Reparation and characterization of microencapsulate dpolythiol. *Polymer*, 2008.

[23] Y.C. Yuan, M.Z. Rong, and M.Q. Zhang. Preparation and characterization of poly (melamine- formaldehyde) walled microcapsules containing epoxy. *Acta Polymerica Sinica*, 2008.

[24] R.S. Jadhav, D.G. Hundiwale, and P.P. Mahulikar. Synthesis and characterization of phenol formaldehyde microcapsules containing linseed oil and its use in epoxy for self-healing and anticorrosive coating. *Journal of Applied Polymer Science*, 2011.

[25] S.H. Cho, H.M. Andersson, S.R. White, N.R. Sottos, and P.V. Braun. Polydimethylsiloxane-based self- healing materials. *Advanced Material*, 2006.

[26] D.S. Xiao, Y.C. Yuan, M.Z. Rong, and M.Q. Zhang. Hollow polymeric microcapsules: preparation, characterization and application in holding boron trifluoride diethyl etherate. *Polymer*, 2009.

[27] A.S. Jones, J.D. Rule, J.S. Moore, N.R. Sottos, and S.R. White. Life extension of self-healing polymers with rapidly growing fatigue cracks. *Journal of the Royal Society Interface*, 2007.

[28] X. Liu, J.K. Lee, S.H. Yoon, and M.R. Kessler. Characterization of diene monomers as healing agents for autonomic damage repair. *Journal of Applied Polymer Science*, 2006.

[29] M.M. Caruso, B.J. Blaiszik, S.R. White, N.R. Sottos, and J.S. Moore. Full recovery of fracture toughness using a nontoxic solvent-based self-healing system. *Advanced Functional Materials*, 2008.

[30] B.A. Beiermann, M.W. Keller, and N.R. Sottos. Self-healing flexible laminates for resealing of puncture damage. *Smart Materials and Structures*, 2009.

[31] A.V. Baglea and R.S. Jadhava. Controlled release study of phenol formaldehyde microcapsules containing neem oil as an insecticide. *International Journal of Polymeric Materials and Polymeric Biomaterials*, 2013.

[32] S.J. Garcia, H.R. Fischer, P.A. White, and A.E. Hughes. Self-healing anticorrosive organic coating based on an encapsulated water reactive silyl ester: Synthesis and proof of concept. *Progress in Organic Coatings*, 2011.

[33] M.X. Huang and J.L. Yang. Facile microencapsulation of hdi for self-healing anticorrosion coatings. *Journal of Materials Chemistry*, 2011.

[34] S.H. Cho, S.R. White, and P.V. Braun. Self-healing polymer coatings. *Advanced Material*, 2009.

[35] D. Kowalskia, M. Uedaa, and T. Ohtsukaa. Self-healing ability of conductive polypyrrole coating with artificial defect. *ECS Transaction*, 2009.

[36] K. Aramaki and T. Shimura. Protection of passivated iron against corrosion in a 0.1 m nano3 solution by coverage with an ultrathin polymer coating of carboxylate sam. *Corrosion Science*, 2009.

[37] A. Yabuki and M. Sakai. Self-healing coatings of inorganic particles using a ph-sensitive organic agent. *Corrosion Science*, 2011.

[38] A. Yabuki, W. Urushihara, J. Kinugasa, and K. Sugano. Self-healing properties of tio2 particle polymer composite coatings for protection of aluminum alloys against corrosion in seawater. *Materials and Corrosion*, 2011.

[39] A .Yabuki and T. Nishisaka. Self-healing capability of porous polymer film with corrosion inhibitor inserted for corrosion protection. *Corrosion Science*, 2011.

[40] Y. Gonzalez-Garcia, J.M.C Mola, and T. Muselleb. Secm study of defect repair in self-healing polymer coatings on metals. *Electrochemistry Communications*, 2011.

[41] S. Neema, M. Selvaraj, and J. Raguraman. Investigating the self healing process on coated steel by svet and eis techniques. *Journal of Applied Polymer Science*, 2013.

[42] A. Kumara and L.D. Stephenson. Self-healing coatings for steel. *Progress in Organic Coatings*, 2006.

[43] M. Zheludkevich and D.G. Shchukin. Anticorrosion coatings with self-healing effect based on nanocontainers impregnated with corrosion inhibitor. *Chemistry of Meterial*, 2007.

[44] D.G. Shchukin and M. Zheludkevich. Layer-by-layer assembled nanocontainers for self-healing corrosion protection. *Advanced Material*, 2006.

[45] D.G. Shchukin, S.V. Lamaka, and K.A. Yasakau. Active anticorrosion coatings with halloysite nanocontainers. *Physical Chemistry*, 2008.

[46] M.L. Zheludkevich and S.K. Poznyak. Active protection coatings with layered double hydroxide nanocontainers of corrosion inhibitor. *Corrosion Science*, 2010.

[47] E.J. Simmons. Use of the pearson bridge in corrosion inhibitor evaluation. *Corrosion*, 1955.

[48] R.V. Sllod and T.E. Larsen. Measurement of the instantaneous corrosion rate by means of polarization data. *Corrosion*, 1957.

[49] K.F. Bonhoeffer, W. Jena, and Z. Elektrochem. The electromotive behavior of iron. *Elektrochem*, 1951.

[50] M. Stern and A.L. Geary. Electrochemical polarization i. a theoretical analysis of the shape of polarization curves. *Journal of the Electrochemical Society*, 1957.

[51] M. Stern. A method for determining corrosion rates from linear polarization data. *Corrosion*, 1958.

[52] K. Aramaki. Protection of iron corrosion by ultrathin two-dimensional polymer films of an alkanethiol monolayer modified with alkylethoxysilanes. *Corrosion*, 1999.

[53] K. Aramak. Self-healing mechanism of an organosiloxane polymer film containing sodium silicate and cerium (iii) nitrate for corrosion of scratched zinc surface in 0.5 m nacl. *Corrosion Science*, 2002.

[54] K. Aramak. Self-healing protective films prepared on zinc by treatments with cerium(iii) nitrate and sodium phosphate. *Corrosion Science*, 2002.

[55] A. Yabuki and K. Okumura. Self-healing coatings using superabsorbent polymers for corrosion inhibition in carbon steel. *Corrosion Science*, 2012.

[56] D. Loveday, P. Peterson, and B. Rodgers. Evaluation of organic coatings with electrochemical impedance spectroscopy. part 2: Application of eis to coatings. *JCT Coatingstech*, 2004.

[57] A. Yabuki, H. Yamagami, and K. Noishiki. Barrier and self-healing abilities of corrosion protective polymer coatings and metal powders for aluminum alloys. *Materials and Corrosion*, 2007.

[58] M.F. Montemor, D.V. Snihirova, M.G. Taryba, and S.V. Lamaka. Evaluation of self-healing ability in protective coatings modified with combinations of layered double hydroxides and cerium molibdate nanocontainers filled with corrosion inhibitors. *Electrochimica Acta*, 2012.

[59] M. Taryba, S.V. Lamaka, D. Snihirova, and M.G.S. Ferreira. The combined use of scanning vibrating electrode technique and micro-potentiometry to assess the self-repair processes in defects on smart coatings applied to galvanized steel. *Electrochimica Acta*, 2011.

[60] D. Snihirova, L. Liphardt, and G. Grundmeier. Electrochemical study of the corrosion inhibition ability of "smart" coatings applied on aa2024. *Journal of Solid State Electrochemistry*, 2013.

[61] A. Pilbth, T. Szab, J. Telegdi, and L. Nyikos. Secm study of steel corrosion under scratched microencapsulated epoxy resin. *Progress in Organic Coatings*, 2012.

[62] R.M. Souto, Y. Gonzlez-Garcia, and S. Gonzlez. In situ monitoring of electroactive species by using the scanning electrochemical microscope. application to the investigation of degradation processes at defective coated metals. *Corrosion Science*, 2005.

[63] D. Kowalski, M. Ueda, and T. Ohtsuka. Self-healing ion-permselective conducting polymer coating. *Journal of Material Chemistry*, 2010.

[64] R. Solmaz, G. Kardas, M. Culha, B. Yazici, and M. Erbil. Investigation of adsorption and inhibitive effect of 2-mercaptothiazoline on corrosion of mild steel in hydrochloric acid media. *Electrochimica Acta*, 2008.

[65] J.D. Rule, E.N. Brown, N.R. Sottos, and S.R. White. Wax-protected catalyst microspheres for efficient eelf-healing materials. *Advanced Material*, 2005.

[66] A. Pizzi. In wood adhesives. *Chemistry and Technology*, 1983.

[67] Sigma-Aldrich. Msds of dimethylethnolamine, 2014.

[68] Sigma-Aldrich. Msds of dicyclopentadiene, 2014.

[69] Sigma-Aldrich. Msds of boiled linseed oil, 2014.

[70] Sigma-Aldrich. Msds. of 3-mercapto trimethoxysilane, 2014.

[71] A. C. Ugural and S. K. Fenster. *Advanced Mechanics of Materials and Applied Elasticity*. Prentice Hall, 2011.

[72] T. Yin, M.Z. Rong, M.Q. Zhang, and G.C. Yang. Self-healing epoxy composites-preparation and effect of the healant consisting of microencapsulated epoxy and latent curing agent. *Composites Science and Technology*, 2007.

[73] Y.C. Yuan, M.Z. Rong, M.Q. Zhang, and J. Chen. Self-healing polymeric materials using epoxy/mercaptan as the healant. *Macromolecules*, 2008.

APPENDICES

A. POLYURETHANE MICROCAPSULE SYNTHESIS SOP

A.1 Make Urethane Prepolymer

1. 250 mL round-bottomed flask, put a stirrer inside
2. Add 142 g cyclohexanone into flask
3. Add 22 g TDI(toluene 2,4-diisocyanate) into flask, stir to completely mixed
4. Add 5mL DAA (1,4-butanediol) at 5 mL min1 using a syringe pump while stirring (use acid buret at maximum speed), making sure M(TDI):M(DAA) < 2.3 to avoid gel
5. React at 80 °C for 24hr with stirring
6. Evaporate under vacuum at 100 °C to evaporate cyclohexanone (stop stirring)

A.2 Determine Percentage of Prepolymer in Specimen

7. Prepare a 250 mL Erlenmeyer flask
8. Weigh to 0.1 g a specimen containing approximately 1.1 milliequivalents of NCO
9. Add 25 mL of dry toluene, place a stopper in the flask, and swirl by hand or on a mechanical agitator to dissolve the prepolymer. This process can aided by warming on a hot plate
10. Use a pipet, add 25 mL of 0.1 N di-n-butylamine solution and continue swirling for 15min with stopper in place
11. Add 100 mL of isopropyl alcohol and 4 to 6 drops of bromphenol blue indicator solution. Titrate with 0.1 N hydrochloric acid to a yellow end point
12. Run a blank titration including all reagents above except prepromer
13. Calculate the percentage of prepolymer

$$NVO\% = \frac{(B - V) \times N * 0.042}{W} \times 100 \quad \text{(A.1)}$$

B = volume of HCl for titration of the blank, mL,

V = volume of HCl for titration of the specimen, mL,

N = normality of HCl,

0.0420 = milliequivalent weight of the NCO group, and W = grams of specimen weight,g

Note: Make 0.1% bromphenol blue indicator solution: mixing 0.10 g of acid, nonwater soluble bromphenol blue with 1.5 mL of 0.1 N sodium hydroxide solution and diluting to 100mL with distilled water

A.3 Make Microcapsule (use DBTL as example)

14. 150 mL beaker, Setup ring and stirring, Set stirring
15. Add chlorobenzene(with 3 g urethane prepolymer and 1 g DBTL) solution
16. Add 28.8 g gum Arabic water solution
17. Stir 30 min for everything to dissolve at 70 °C
18. Add 30%(vs prepolymer) ethylene glycol (chain extender) 5 mL.min1
19. Stir 2 h at 1000 rpm at 70 °C
20. Filter and dry
21. If capsule are sticky together, re-dissolve them, add EMA and filter again

B. UREA-FORMALDEHYDE MICROCAPSULE SYNTHESIS SOP

1. Clean a 600 ml beaker
2. Add to ring stand so that it is suspended just above bottom of water bath
3. Clean stirring rod (sharp blade rather than propeller)
4. Add to stirring stand so blades is just above bottom of beaker
5. Add 200 mL of de-ionized water to the beaker
6. Add 50 mL of 2.5 wt% PVA
7. Set mixer between 300-600rpm depending on desired size of microcaps
8. Tare small weighing dish
9. Add 5.0 g of Urea
10. Add 0.5 g of ammonium chloride
11. Add 0.5 g of resorcinol
12. Rinse pH meter in de-ionized water
13. Adjust pH meter to 7 while immersed in standard solution
14. Rinse pH meter with de-ionized water
15. Adjust pH meter to 4 while immersed in second standard solution
16. Rinse pH meter with de-ionized water
17. Open NaOH, HCl and Octanol bottles, prepare 3 pipets
18. Submerse pH meter in solution and hold until pH adjustment is complete
19. Add NaOH to bring pH above 3.5 (3.6-3.8)
20. Add HCl to bring pH back to 3.5 (1 drop = 0.1 pH)
21. Add 1 (to 2) drops of Octanol to remove bubbles
22. Add 60 mL of distilled healing agent
23. Wait 10 minutes for everything to dissolve (especially Urea)
24. Tare a 20 mL vial on the scale
25. Use 20 mL a vial to weigh 12.667 g of formaldehyde and add it to solution

26. Cover beaker with foil

27. Set target temperature at 55 °C at 1 °C/min or 60 °C/hour

28. Set timer for 4 hours

29. Allow pipettes and 20mL vial to dry in hood and then dispose them in sharp-waste can

30. Remove stirring rod

31. Wash off stirring rod with de-ionized water into microcapsule beaker

32. Clean ceramic filter/glass funnel combination

33. Place filter on large drainage jar in hood and slowly pour in microcapsules

34. If filtering is clogging, switch to coarser paper filter with ceramic funnel

35. Apply shop vacuum to drainage jar

36. When drained, empty microcaps into baking pan, cover with paper towel and allow to air dry overnight

C. PHENOL-FORMALDEHYDE MICROCAPSULE SYNTHESIS SOP

1. Prepare 400 ml beaker
2. Add 150 ml de-ionized water into beaker
3. Add stirring blades and set stirring speed at a certain rate
4. Add 5 ml 5% wt% PVA
5. Add 3.76 g phenol
6. Add 0.5 g ammonium chloride
7. Adjust pH to 7 using ammonia
8. Add 25 ml linseed oil and stabilize the solution under agitation for 30mins
9. Add 6.486 g 37% formaldehyde
10. Stir 2 hr with 250 rpm under 65 °C
11. Adjust pH back to 3 via 5% wt% HCl
12. Add 0.5 g resorcinol
13. React for 2.5 hr under 65 °C
14. Filter and rinse with water and xylene
15. Dry

D. MELAMINE-UREA-FORMALDEHYDE MICROCAPSULE SYNTHESIS SOP

D.1 Preparing Melamine-Formaldehyde Pre-polymer

1. Prepare 150 mL beaker, put a stirrer inside
2. Add 70 ml distilled water
3. Add 3.81 g Melamine
4. Add 9.55 g formaldehyde
5. Keep reaction under 70 °C for 25mins (until everything dissolves)

D.2 Making Microcapsules with Linseed Oil

6. repare 400 ml beaker
7. Add 200 mL of de-ionized water to the beaker
8. Add 10ml 5% wt% PVA into above beaker
9. Add stirring blades just above bottom of beaker and set stirring speed at 500 rpm
10. Add 0.84 g urea
11. Add 0.5 g ammonium chloride
12. Add 0.5 g resorcinol
13. Adjust pH to 3.5 using pH meter
14. Add 50 ml linseed oil
15. Add MF-prepolymer synthesized earlier
16. Adjust pH to 3.5 again using HCL or NaOH solution
17. Keep reaction for 4hr under 55 °C using water bath
18. Wash and dry

E. THE COMPLETE CIRCUIT OF DAQ PROGRAM

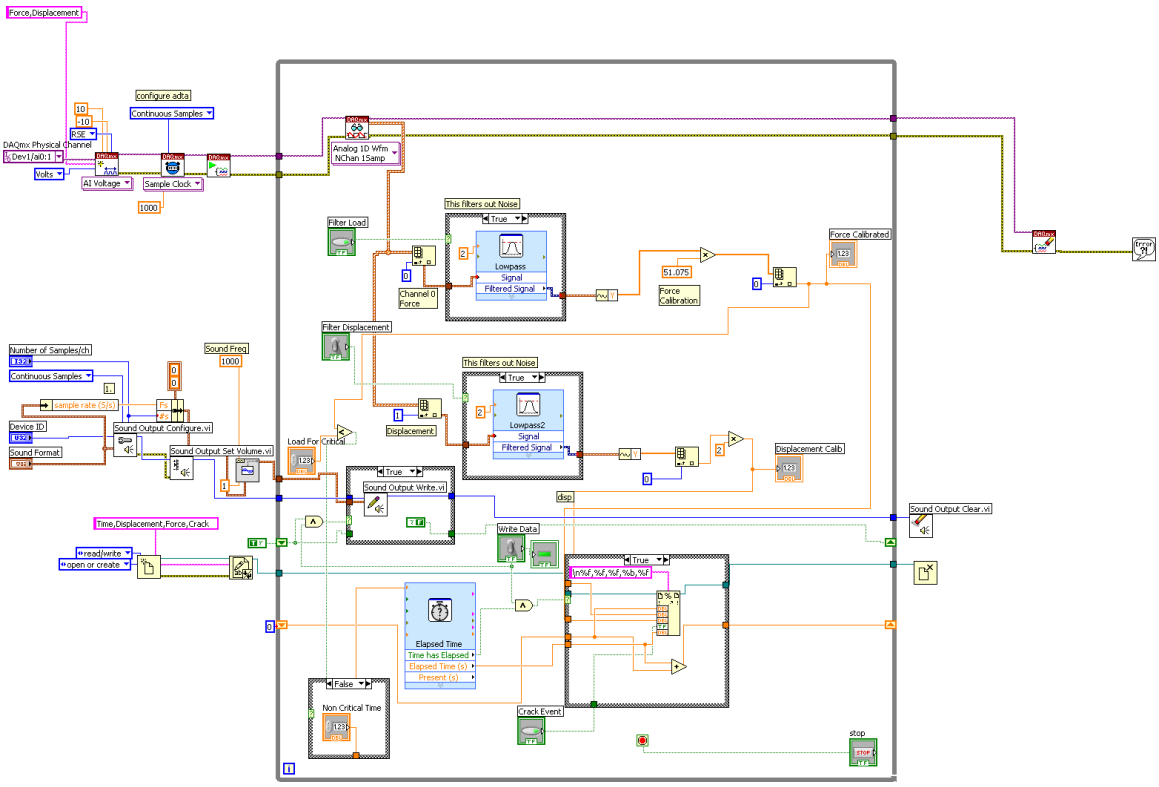

Figure E.1. The Complete Circuit of DAQ Program